ORIGINAL PAPER



Effect of Al₂O₃ Support on Co-Based SiO₂ Core–Shell Catalysts for Fischer–Tropsch Synthesis in 3D Printed SS Microchannel Microreactor

Meric Arslan¹ · Sujoy Bepari² · Richard Abrokwah² · Nafeezuddin Mohammad^{2,3} · Juvairia Shajahan³ · Debasish Kuila^{1,2,3}

Accepted: 17 October 2022

© The Author(s), under exclusive licence to Springer Science+Business Media, LLC, part of Springer Nature 2022

Abstract

Fischer Tropsch Synthesis (FTS) using syngas, a mixture of carbon monoxide (CO) and hydrogen (H₂), obtained from renewable sources in the presence of a catalyst, is an excellent route to long-chain hydrocarbons and fuels. In this study, cobaltmesoporous silica catalysts for FTS were prepared by two procedures-Co@SiO₂ at 200 °C, and high pressure in an autoclave (AC), Co@SiO₂ (One Pot or OP) at room temperature and 1 atm; the effect of Al₂O₃ on Co-SiO₂ as Co@SiO₂Al₂O₃ (One Pot or OP) core-shell catalysts was investigated for FTS at 20 bar in 3D printed stainless steel (SS) microchannel microreactors. These catalysts were characterized by different techniques such as N₂ physisorption, XRD, SEM, TEM, H₂-TPR, TGA-DSC, and XPS. The N₂ physisorption studies show that the BET surface area of Co@SiO₂ (Autoclave) is much higher than that of Co@SiO₂ (One Pot), and the surface area decreases upon the addition of Al₂O₃ to yield Co@SiO₂Al₂O₃ (OP) catalyst. In TPR analysis, the Co@SiO₂ (OP) based catalyst had much higher reduction temperature than the Co@SiO₂ (AC) catalyst. The XRD analysis shows that the Co@SiO₂ (Autoclave) based catalyst is more crystalline when compared to other catalysts. The TEM and SEM images revealed agglomerations in the case of Co@SiO₂(OP) and Co@SiO₂Al₂O₃(OP) based catalysts. The TGA analyses of as-synthesized catalysts, before calcination, showed good stability of the catalysts. The oxidation state and binding energy of all catalysts, evaluated by XPS analysis, show a significant shift based on the catalyst preparation. All F-T reactions were carried out in a 3D-printed SS microreactor at 20 bars in the temperature range of 200–370 °C with H₂/ CO molar ratio of 2:1. The highest CO conversion for Co@SiO₂ AC, Co@SiO₂Al₂O₃ OP, Co@SiO₂ OP are 85%, 45%, and 27% respectively. The highest selectivity to C₄₊% was observed for Co@SiO₂ AC in SS Microreactors in the temperature range of 200–300 °C, and the % selectivity for the C_{4+} follows the order: $Co@SiO_2AC > Co@SiO_2Al_2O_3OP > Co@SiO_2OP$.

Published online: 03 December 2022



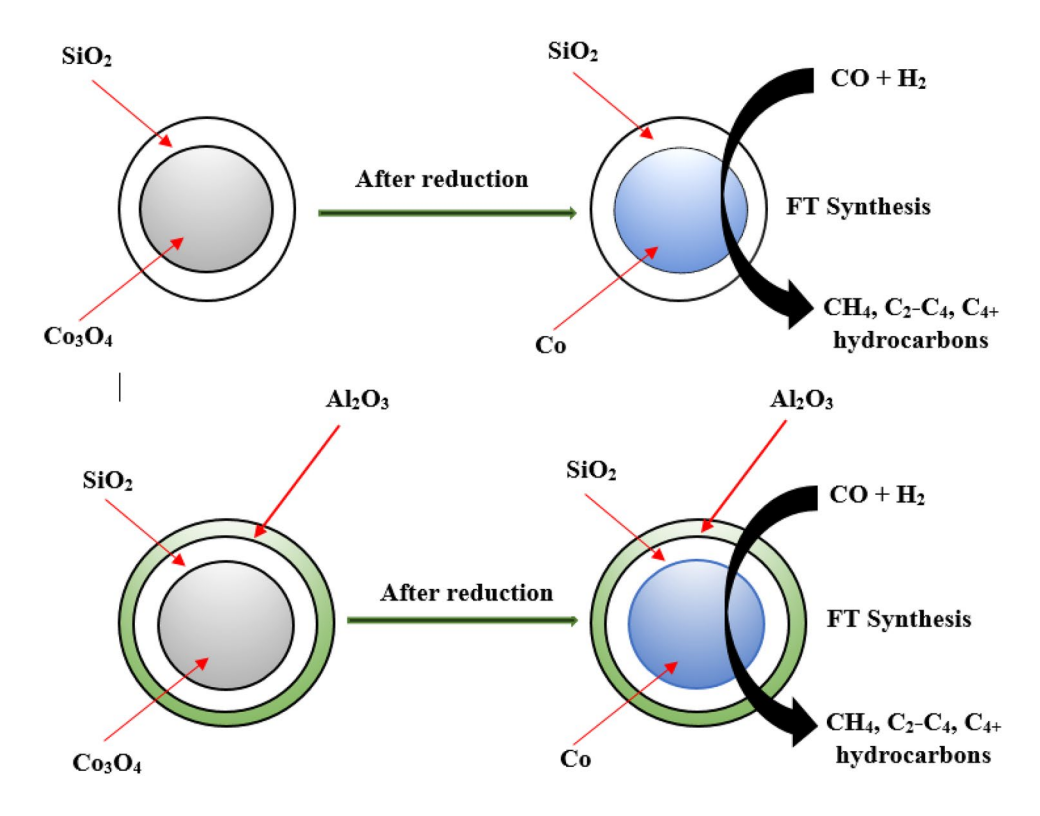
Debasish Kuila dkuila@ncat.edu

Department of Applied Science and Technology, North Carolina Agricultural and Technical State University, Greensboro, NC 27411, USA

Department of Chemistry, North Carolina Agricultural and Technical State University, Greensboro, NC 27411, USA

Joint School of Nanoscience and Nanoengineering, North Carolina Agricultural and Technical State University, Greensboro, NC 27411, USA

Graphical Abstract



 $\textbf{Keywords} \ \ FT \ synthesis \cdot Stainless \ steel \ microreactor \cdot Co \ catalyst \cdot Mesoporous \ composite \ oxide \cdot Silica \cdot Silica \cdot alumina \ support$

1 Introduction

Conversion of synthesis gas, a mixture of H₂ and CO, to hydrocarbons over different metal catalysts was discovered by Franz Fischer and Hans Tropsch at Kaiser Wilhelm Institute for Coal Research in Mulheim in 1923 [1, 2]. This process is widely known as Fischer-Tropsch synthesis (FTS). They conducted CO hydrogenation over iron, cobalt, and nickel catalysts in a temperature range of 180-250 °C and 1 atm pressure to produce linear hydrocarbons in the product mixture. The feedstock of the syngas is mainly derived from the gasification of various solid carbonaceous resources like coal and biomass, and are used in many chemical industries for the production of transportation fuels. Indeed, the depletion of petroleum resources and the abundant use of natural resources like gas and coal has gained much industrial research interest for alternative technologies to produce fuels like Fischer-Tropsch Synthesis. Conversion of gas (Gas-To-Liquid) and coal (Coal-To-Liquid) to hydrocarbons are currently the foremost promising routes to supply environmentally friendly clean fuels [3].

For commercial production of liquid fuels, iron and cobalt are employed in the temperature range of 200 to 300 °C

and at pressure > 10 bar [4, 5]. Thus, current catalysts used for FTS are cobalt, iron, and more recently, ruthenium loaded on various supports [6-8]. Cobalt-based catalysts are highly active but sensitive to poisoning, even when a small amount of sulfur-containing compound is present. The reaction conditions for ruthenium catalysts are milder due to their considerable high activity. However, its high price and limited resource hinder its industrial application. Iron-based catalysts are attractive due to their low price, abundant resources, tunable properties, and controllable selectivity toward various hydrocarbons. Various technologies have been investigated to engineer the conventional iron-based catalyst for FTS to promote the activities and manipulate the product distribution. It includes the modification of the support properties, employment of favorable composites, addition of various promoters, alteration of the activation methods, synthesis method, etc. In this study, we have used a microreactor for FTS synthesis. Microreactor, as the name implies, is a very small device containing one or several microchannels with inlet and outlet flow regions [9, 10]. They are termed 'Lab-on-a-chip' devices since the size is very small. The reaction zones are the microchannels through which fluid or the reactants flow for a reaction to



take place. In addition, these microreactors enable higher throughput experiments with fewer reactants, fewer utilities, and safety advantages compared to the standard reactors used for research [11]. The lower reaction volumes of microsystems that undergo high heat and mass transfer rates help reactions to occur more aggressively with higher yields that are generally achieved by conventional reactor technology [12]. Moreover, new reaction kinetics [13], hydrodynamics, and difficult reaction pathways are easy to carry out in a confined small volume [1] compared to conventional chemical reactors [14]. Since the reaction volumes are very small compared to the standard reactors, it is much safer to conduct chemical reactions that form highly reactive intermediates during the chemical process. These inherent safety characteristics of microreactors are advantageous for shipping the toxic and highly reactive intermediates to safe storage and analysis locations.

One of the important characteristics of microreactors is large surface areas, and their inherent safety can be utilized to scale up by stacking them together. This scale-up strategy makes it feasible to switch from the formation of micro products to macro products without much loss of reactivity [15, 16]. Moreover, the utilization of the continuation process by microflow systems eliminates the batch-to-batch variations in product quality and maintains the reaction parameters precisely [17]. The design selection of the microreactor and the material used for its fabrication depends on the intended chemical applications [9]. Classical chemical reactions can be carried out by using stainless steel, glass, silicon, polymers, and Stainless steel (SS) microreactors. The applications are mainly supported by large-scale chemical production [18], whereas glass [19], polymer [20] silicon are more attractive for laboratory applications. Polymer microreactors are mainly fabricated using PDMS (Polydimethylsiloxane) [21].

In this work, we have used SS microreactors to investigate the performance of cobalt-based catalysts with an attempt to prepare possible core—shell structure and studied the effect of physical and chemical properties of the catalysts on Fischer—Tropsch Synthesis. The catalysts were prepared by two different procedures: autoclave (AC) and one pot (OP), to investigate the effect of preparation on catalytic activity. While the synthesis of catalysts in an autoclave was carried out at 200 °C and high pressure, the OP preparation was done at room temperature under normal conditions. More significantly, we tested the effect of mixed support by incorporating Al₂O₃ on SiO₂. The comparative stability studies of Co@SiO₂ (AC), Co@SiO₂ (OP) and Co@Al₂O₃-SiO₂ (OP) catalysts for FT Synthesis in SS Microchannel Microreactor were investigated.

2 Experimental Methods

2.1 Materials

The reagents used for catalyst synthesis were of analytical grade with no further purification. Tetraethyl orthosilicate, 99% (TEOS) and ammonium hydroxide, ACS (American Chemical Society) reagents, were purchased from Acros Organics, New Jersey, USA. Cetyltrimethylammonium-bromide (CTAB), Co (NO₃)₂.6H₂O, Fe (NO₃)₃·9H₂O were purchased from Sigma Aldrich. Ethanol (anhydrous) and acetone, ACS grade, were obtained from Fisher Scientific, New Jersey, USA.

2.2 Catalyst Synthesis and Loading

2.2.1 Catalyst Synthesis (One-Pot)

Cobalt-based nanocatalysts supported by SiO₂ and Al₂O₃ were synthesized using a one-pot hydrothermal procedure [22]. TEOS, CTAB, de-ionized water, and ethanol were used. The quantity of metal precursor was calculated based on the weight percentage of metal to be incorporated into the catalysts. Typically, the weighed surfactant (CTAB) was dissolved in de-ionized water at 30 °C and stirred until the solution became clear. A separate solution was prepared by dissolving metal precursors in ethanol and stirring it for approximately 30 min. The dissolved metal solution was gently poured into the CTAB solution and stirred vigorously for 30 min. TEOS, the limiting reagent for this chemical synthesis, was added dropwise into the mixture while stirring continuously for another 30 min. To precipitate the metal hydroxides at a pH of about 9-11, ammonium hydroxide was added dropwise to the solution under stirring. The mixture was then stirred for another 3 h, followed by aging for 18 h at 65 °C. The precipitate was washed with de-ionized water until it reached a pH of 7, then rinsed with ethanol and filtered. The filtered material was dried in the air for 24 h and then dried in an oven at 98 °C for 24 h. This was followed by calcination at 550 °C for 6 h with a heating rate of 2 °C/min to remove the CTAB surfactant. It was then cooled to room temperature. The catalysts were also synthesized with SiO₂ and Al₂O₃ supports. They are labeled as Co@SiO₂(one pot) and Co@SiO₂Al₂O₃ (one pot) in this study.

In addition, the Co@SiO₂ (Autoclave) catalyst was prepared in a stainless-steel autoclave using 4.5 g of polyvinylpyrrolidone (PVP) and 2 g of Co (NO₃)_{2.6}H₂O, dissolved in 300 ml ethanol with magnetic stirring. The solution was transferred to stainless steel autoclave, sealed, and then heated at 180 °C for 4 h when a black suspension was obtained.



The pore diameter of the silica shell was controlled by the addition amount of a swelling agent, trimethyl benzene (TMB). The synthesis method is as follows; Mixture A was prepared by mixing 120 g of water, 14 g of cetyltrimethylammonium chloride (CTACl), and 3.36 ml of 1,2,4-trimethylbenzene (TMB) as a swelling agent to obtain the final mixture with the tetraethylorthosilicate (TEOS) mole ratios of 0.6. The mixture was heated up to 60 °C under stirring for 30 min. The black suspension of Co₃O₄ nanoparticles encaged by polyvinylpyrrolidone (PVP) shell prepared in the first part was added dropwise to the above surfactant solution, and the whole mixture (mixture A) was stirred for another 3 h.

In another autoclave, mixture B was prepared by mixing 10 ml of tetraethylorthosilicate (TEOS) and 75 ml of triethanolamine (TEA). This mixture was placed in a stainless steel autoclave and heated in an oven at 90 °C for 20 min. This mixture B was added to mixture A at room temperature, and the resulting mixture was magnetically stirred for 48 h at 600 rpm. The product was then collected by filtration, washed thoroughly with distilled water and ethanol, and then dried at 60 °C. The dried product was then calcined at 500 °C for 6 h in the air.

2.3 Catalyst Activity Test

The FT experiments were conducted in an in-house-built LabVIEW automated experimental setup with precise control of the operating conditions. The experimental setup is shown in Fig. 1. The volumetric flow rate of the syngas mixture (H₂ &CO) was controlled by a pre-calibrated mass flow controller (Bronkhorst) with a maximum rate of 20 sccm. The carrier gas and nitrogen were controlled by a precalibrated mass flow controller (Aalborg) with a maximum flow of 20 sccm. The pressures upstream and downstream were monitored by Bronkhorst pressure gauges, from which the information was fed to an Aalborg solenoid valve, which controlled the reaction pressure. The Labview 2018 program automated the whole setup. Agilent Technologies 7890B GC and Agilent 5977 MSD systems were used for

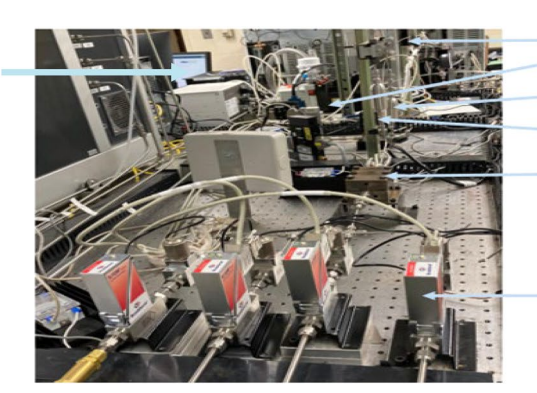
the qualitative and quantitative analysis of the reaction products. Prior to experiments, the catalyst inside the microreactor was reduced in-situ at 350 °C overnight to compensate for the losses in ex-situ reduction via oxidation of catalyst before reaction. The FT reaction was performed with syngas ($H_2/CO=2$) using a fixed gas hourly space velocity (GHSV = 12,000 h⁻¹). The H_2 and CO flow rates were maintained at 4 and 2 ml/min, respectively. The N_2 flow rate was maintained at 1.5 ml/min.

2.4 Catalyst Characterization

N₂ adsorption-desorption isotherm of all catalysts was measured by the BET surface area analyzer (Model: 3Flex, Make: Micromeritics, USA) instrument at constant liquid N_2 temperature (- 196 °C). The surface area and pore size distributions were calculated by N2 adsorption-desorption isotherm using the Brunauer-Emmett-Teller (BET) and Barrett-Joyner-Halenda (BJH) method. The X-ray diffraction was carried out using a powder X-Ray diffractometer (Model: Bruker AXS). The detection limit of the instrument was in the range of 10–80° with a step interval of 0.02° using a Cu Kα1 radiation source with a wavelength of 1.5406 Å. Peaks derived from these spectra were used to identify the metals, their oxidation state, and their morphology. Temperature programmed reduction was performed using a chemisorption analyzer (Model: 3Flex, Make: Micromeritics, USA). 0.05 g of sample material was measured and placed into a chemisorption tube on top of a covering layer of quartz wool beneath a quartz filter cap upon which the sample was placed. The sample was then placed under a 10% H₂/Ar (1:9 wt %) flow of 50 ml/min and a ramp rate of 10°C/min from room temperature to 800 °C to determine the reducibility of the metal oxides. Synthesized materials were imaged using a ZEISS Auriga Focused Ion Beam Scanning Electron Microscope (FIB-SEM) at the Joint School of Nanoscience and Nanoengineering. These images were used to conclude the average particle size, morphology, and topography of each catalyst. The Transmission Electron Microscopy (TEM) was carried out by Thermo Fischer Talos (Model: F200X).

Fig. 1 Experimental setup for FT Synthesis

LabView



Backpressure controller

Cold trap

Reactor and heating block

MFCs for CO2, N2, CO & H2



The field emission system was operated at 200 kV. The decomposition temperature of polymer templates used in the mixed composite support preparation was determined by Thermogravimetry and Differential scanning Calorimetry (TGA–DSC) (Model: TA instruments, New Castle, DE, USA). The samples were heated to 1000 °C at a heating rate of 10 °C/min. The analysis was done in presence of Air at 100 ml/min. The oxidation states of all catalysts were determined by X-ray photoelectron Spectroscopy (Model: Escalab Xi+-, Make: Thermo Scientific, West Sussex, UK).

3 Results and Discussion

3.1 Experimental Details of Core-Shell Catalyst

Co@SiO₂ and Co@Al₂O₃-SiO₂ catalysts were prepared using the autoclave and one-pot synthesis procedures. These catalysts were characterized by a series of techniques, N₂ physisorption, XRD, SEM, TEM, H₂-TPR, TGA-DSC, and XPS. The expected phase was confirmed, and the core-shell structure was observed. The effect of outer shell type on the properties of the catalysts was also investigated.

3.2 Characterization Techniques

3.2.1 Brunauer Emmett Teller (BET) Analysis

The textural properties of the Co@SiO₂ (AC), Co@SiO₂ (OP), and Co@SiO₂Al₂O₃ (OP) catalysts were determined by the N₂ physisorption technique. In Fig. 2a, the N₂ adsorption-desorption isotherm of Co@SiO₂ (OP) catalyst shows a typical type-IV isotherm with a long hysteresis loop and capillary condensation occurred at a relative pressure (P/ P_0) of 0.4–1.0, which is characteristic of mesoporous materials according to the classification of International Union of Pure and Applied Chemistry (IUPAC). The isotherm of the Co@SiO₂Al₂O₃ (OP) catalyst belongs to type IIb with a type H3 hysteresis loop and capillary condensation characteristic of the existence of inter-particle pores in aggregates [23]. This result is also supported by the SEM micrographs, which show the agglomeration of a large number of small particles [24]. The hysteresis loop suggests the presence of pores with different accesses, and they are not uniform. Figure 2b shows the Co@SiO₂ (AC) catalyst has a type-IV isotherm with a hysteresis loop according to the IUPAC classification. No capillary condensation is observed in this case, which suggests that the catalyst synthesis method plays an important role. Figure 2c shows the pore size distribution (PSD) of the catalysts. Both Co@SiO₂ (OP) and Co@SiO₂Al₂O₃ (OP) catalysts exhibit similar pore sizes of 3.9 nm with a very low contribution to the larger pore sizes, corresponding to secondary mesoporosity. In the case of the

 $Co@SiO_2$ (AC) catalyst, the average pore size is 3.6 nm, and it is mesoporous.

Table 1 summarizes the BET surface area, pore volume, and average pore sizes of all catalysts. The surface area and pore volume are lower for Co@SiO₂ (OP) when it was compared to that of Co@SiO₂ (AC). This is probably due to the catalyst preparation method. Surface area and pore volume decreased significantly for Co@SiO₂Al₂O₃ (OP) material. This is due to a combination of Al₂O₃ and mesoporous SiO₂, similar to that reported before [25].

3.2.2 X-Ray Diffraction Studies (XRD) Analysis

XRD studies were carried out to obtain information about the crystalline nature of the catalysts. The mesoporous nature of the support was confirmed from N_2 adsorption Type IV isotherms as shown in Fig. 4 and is consistent with the results of powder XRD studies. The wide-angle XRD analysis was carried out for different catalysts.

Figure 3 shows the XRD patterns of different catalysts. The broad peak around 22° belongs to mesoporous SiO_2 [25, 26]. The diffraction peaks at various 20 values such as 18.72° , 22.82° , 32.94° , 38.70° , 45.06° , 60.18° , and 65.02° correspond to Co_3O_4 with cubic structure, indicating that Co_3O_4 is the primary crystalline cobalt species, referred to standard JCPDS- 42-1467 database [27]. No noticeable peak is observed for Co_3O_4 in the $Co@SiO_2$ (OP) sample; this suggests that either the metal and metal oxides are amorphous or well dispersed on the surface [28, 29] or present in the lower crystalline from that is not detectable by XRD [30, 31]. The SiO_2 peak disappears in the $Co@SiO_2Al_2O_3$ (OP) XRD spectrum due to the incorporation of Al_2O_3 in the mesoporous silica shell [32].

The average crystal size of the catalysts can be measured from the XRD data using the modified Scherrer equation, and they are shown in Table 2 [33]. While the crystal size of Co3O4 is 11.06 nm in Co@SiO2 (AC), the crystal size of Co3O4 is estimated to be 10.36 nm in Co@SiO2Al2O3 (OP) catalyst. The size of the cobalt oxide nanoparticles decreases by 0.7 nm. Crystallinity differences have been observed in the XRD patterns of Co@SiO2 (AC) and Co@SiO2 (OP). The percentage of crystallinity index was calculated using the following equation [34]

 $CI\% = 100 \times (S_c/S_t)$ where S_c is the area of the crystalline domain and S_t is the area of the total domain.

The crystallinity index percentages of Co@SiO2 (AC) and Co@SiO2 (OP) are 46.22 and 28.30, respectively. This difference in the crystallinity partly accounts for the thermal, chemical properties, and reactivity differences between the samples prepared by two methods. Chu et al. [35], in their study, also showed that the addition of Al2O3 to a core–shell



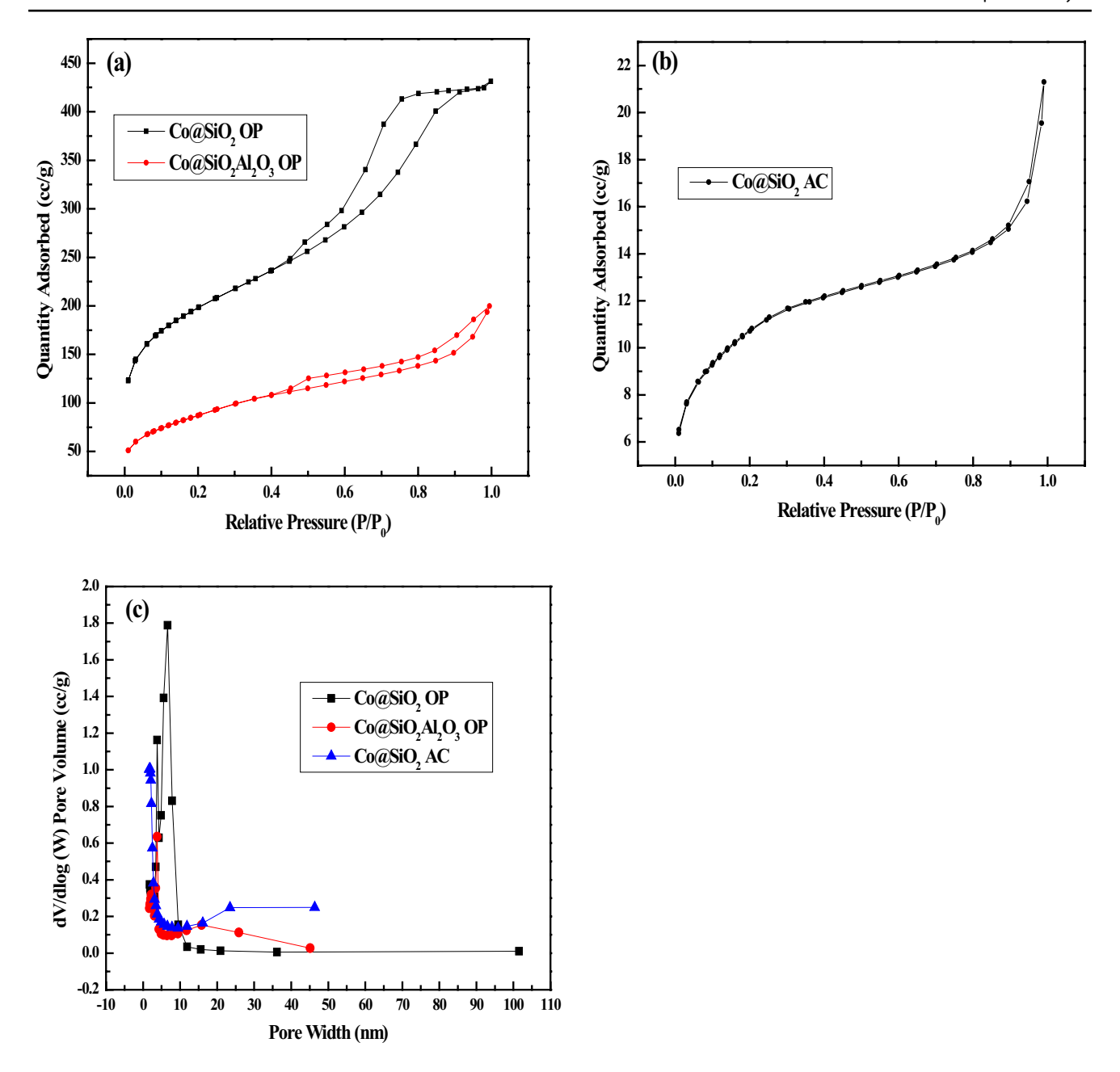


Fig. 2 N_2 Adsorption—desorption isotherms of: a Co@SiO₂ OP and Co@SiO₂Al₂O₃ OP and b Co@SiO₂ AC; c pore size distribution plots of all catalysts

Table 1 BET surface areas, pore sizes and pore volumes of different catalysts

Catalyst	Sp. surface Area (m²/g)	Pore volume (cc/g)	Pore diameter (nm)
Co@ SiO ₂ (AC)	805	0.73	3.6
Co@ SiO ₂ (OP)	670	0.66	3.9
$\mathrm{Co@SiO_{2}Al_{2}O_{3}}\left(\mathrm{OP}\right)$	308	0.30	3.9

structure resulted in the reduction of cobalt nanocrystal size observed in their studies.

3.2.3 Scanning Electron Microscopy (SEM) Analysis

SEM studies were used to investigate the morphology and elemental composition (weight%) of each catalyst. The morphologies of different core—shell catalysts are shown in Fig. 4. It should be noted that silica is a commonly used material in core—shell catalysts because of its mechanical strength, structural characteristics, and ease of carrying out



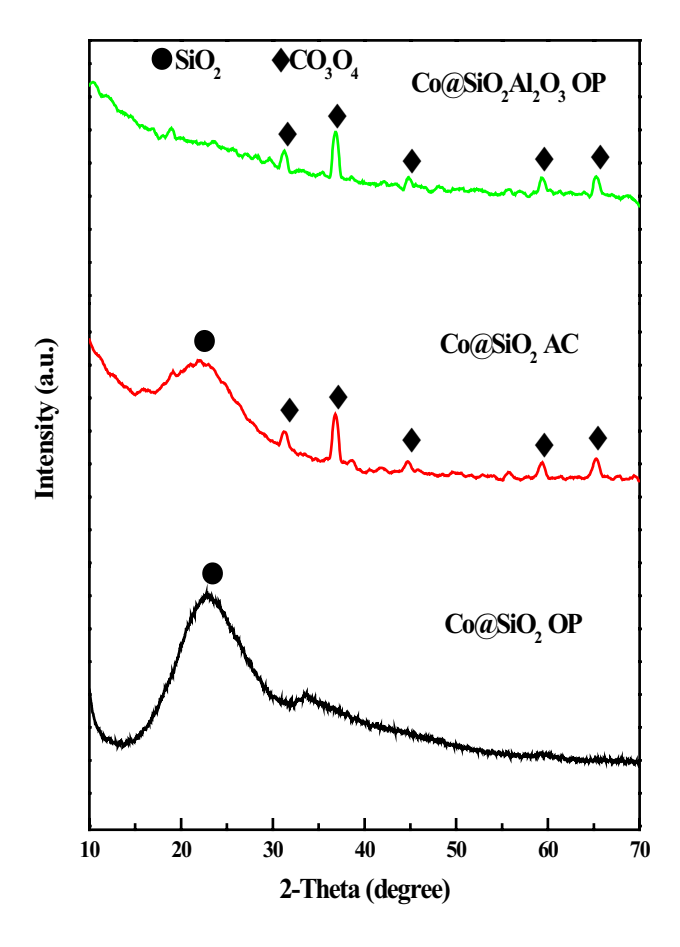


Fig. 3 Wide angle XRD patterns of Co@SiO $_2$ (AC), Co@SiO $_2$ (OP), and Co@SiO $_2$ Al $_2$ O $_3$ (OP) Catalysts

Table 2 Crystal size calculation* based on XRD data

Catalyst	Ave. Co3O4 Crystal Size (nm)
Co@SiO2 (AC)	11.06
Co@SiO2Al2O3 (OP)	10.36

^{*}Using modified Scherrer equation [33]

surface functionalization [31, 32, 36, 37]. It can be observed that the particles are well dispersed for the $Co@SiO_2$ (AC) and $Co@SiO_2$ (OP) catalysts (Fig. 4a and b). However, there is some agglomeration observed for the $Co@SiO_2Al_2O_3$ (OP) catalyst (Fig. 4c). This is most likely due to the incorporation of Al_2O_3 into the mesoporous silica shell. The $Co@SiO_2Al_2O_3$ (OP) samples yielded not only larger particles but also indicated lower adhesion of cobalt to support.

Table 3 shows the energy-dispersive X-ray spectrometry (EDS) results of all catalysts. Co@SiO₂ (AC) and Co@SiO₂ (OP) catalysts mainly contain Co, Si, and O elements. All elements are evenly distributed for these catalysts. However,

in the case of the Co@SiO₂Al₂O₃ (OP) catalyst, the metal loadings changed significantly due to the addition of Al₂O₃. The O element in the EDX analysis is due to the surface oxidation of metals incorporated in the catalyst.

3.2.4 Transmission Electron Microscopy (TEM) Analysis

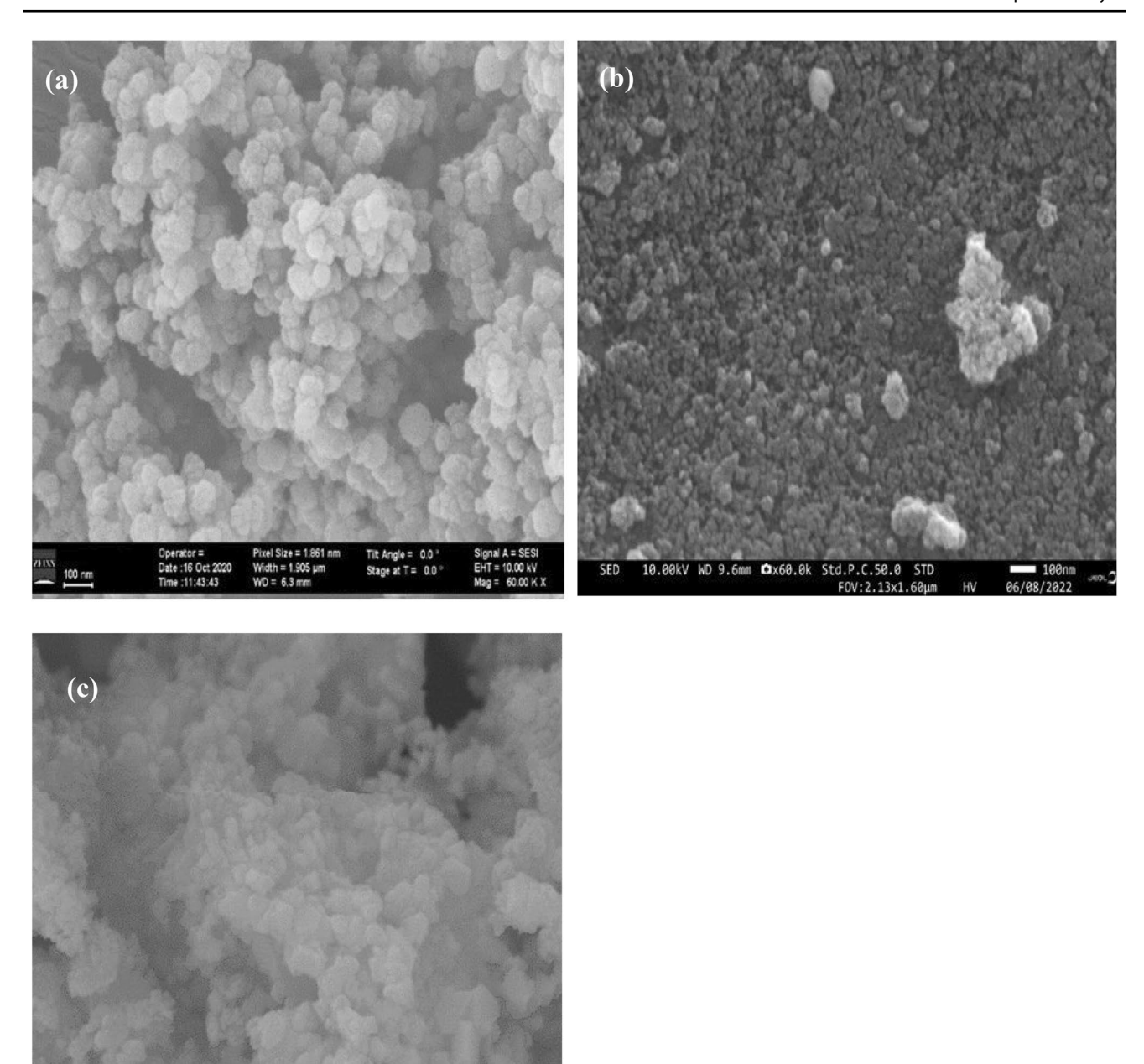
To confirm the presence of core-shell structure, TEM analysis was carried out for all catalysts. The TEM micrographs are shown in Fig. 5. The particle diameter was determined by Image J software. Based on TEM images (Fig. 5a, b, and c), Co@SiO₂ (AC) has a size of 25 nm in the outer diameter with a 2 nm thick silica shell. Co@SiO₂Al₂O₃ (OP) has a size of 33 nm in the outer diameter with 9 nm thick silica and alumina shells. The size of cobalt particles and the thickness of the silica layer both increase with the change in synthesis method, which might suggest that the silica layer suppressed the growth of cobalt particles [25]. When two methods are compared, autoclave synthesis is much better because onepot synthesis bolstered agglomeration (large darker spots) of the metal particles. The mesoporous silica layer acts as an outermost shell and plays a major role in protecting cobalt nanoparticles [38]. The XRD analysis shows that the Co@ SiO₂ (OP) catalyst is predominantly amorphous in nature with minimal crystallinity. Hence, the core-shell structure is not clearly defined in TEM analysis. [See updated supplementary data].

3.2.5 Temperature Programmed Reduction (TPR)

Temperature programmed reduction (TPR) analysis was performed to study the reduction behavior of the metal oxide catalysts to evaluate the metal-support interactions. Figure 6 shows the H_2 -TPR profile of all catalysts.

For the Co@SiO₂ (AC) catalyst in Fig. 6, two main reduction peaks are observed at 347 and 375 °C, respectively. The observed reduction peaks are mainly due to the reduction of the cobalt oxide nanoparticles ($Co_3O_4 \rightarrow CoO \rightarrow Co$). The peak at 440 °C is attributed to the reduction of bulk Co₃O₄ nanoparticles [39]. The reduction of Co³⁺ species to Co²⁺ is followed by the immediate reduction of Co²⁺ to metallic Co⁰ [40, 41]. In the case of Co@SiO₂ (OP) material, a small reduction peak is observed at 344 °C, which might be due to the reduction of Co₃O₄ to CoO. However, a very broad peak is also observed at 833 °C, which may be attributed to the reduction of slightly reducible cobalt silicate species formed during calcination and H2-TPR experiments by reaction of CoO with Si-OH groups of mesoporous SiO2 support [42]. Two successive reduction peaks (386 and 405 °C) are observed for the Co@SiO₂Al₂O₃ (OP) catalyst. These peaks are attributed to the reduction of CO₃O₄ to metallic Co. The broader peak at 672 °C can be attributed to cobalt silicate reduction. This peak is shifted to a lower temperature from





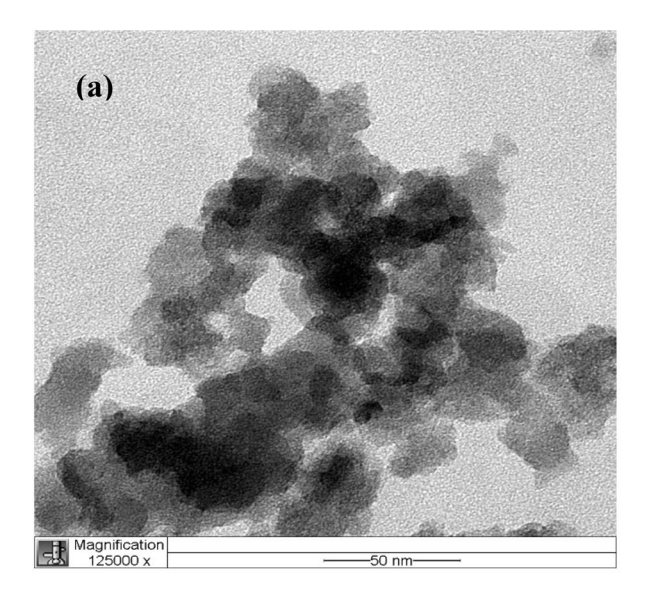
 $\textbf{Fig. 4} \quad \text{SEM images of: } \textbf{a} \ \text{Co@SiO}_2 \ (\text{AC}); \ \textbf{b} \ \text{Co@SiO}_2 \ (\text{OP}); \ \textbf{c} \ \text{Co@SiO}_2 \\ \text{Al}_2 \\ \text{O}_3 \ (\text{OP}) \ \text{catalysts}$

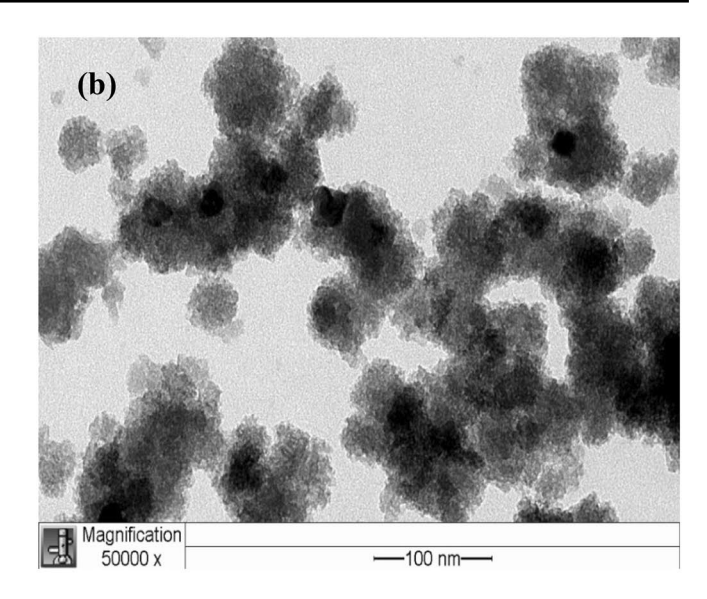
Table 3 SEM-EDS analysis of synthesized catalysts

Catalysts	Metal loading (Wt.%)			
	Co	Si	Al	О
Co@SiO ₂ (AC)	3.02	37.85	_	59.12
Co@SiO ₂ (OP)	6.05	38.46	_	55.48
$\text{Co@SiO}_2\text{Al}_2\text{O}_3 (\text{OP})$	15.44	18.81	11.36	54.39

833 to 672 °C due to the incorporation of Al₂O₃ in the silica shell. Thus, it leads to the weak interaction between Co species with mesoporous silica support. The TPR results suggest that the synthesis method plays an important role in the formation of metal oxide or other species. We speculate that in Co@SiO2 OP, a cobalt silicate species is produced. It is very difficult to reduce cobalt oxide nanoparticles because the silica shell yields higher thickness in a one-pot







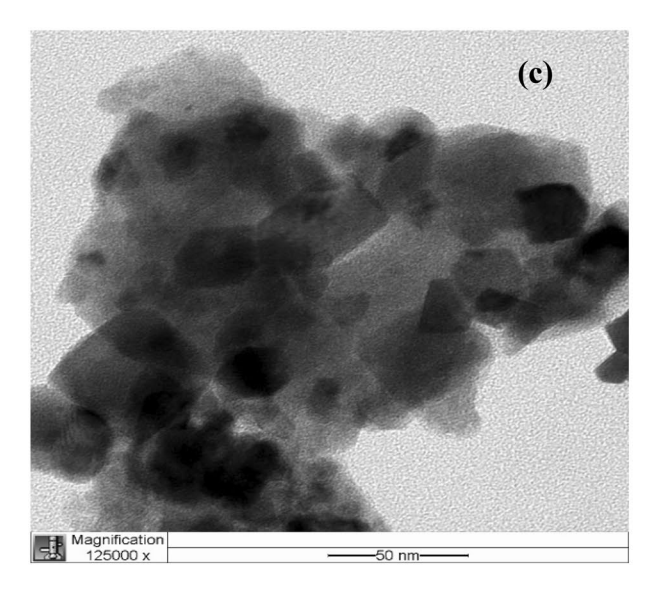


Fig. 5 TEM images of: a Co@SiO₂ (AC); b Co@SiO₂ (OP); c Co@SiO₂Al₂O₃ (OP) catalysts

synthesis. Thus, the TEM analysis is consistent with the results from our TPR studies.

Table 4 shows the amount of H_2 consumption and reduction degree of different synthesized catalysts in our TPR studies. The highest H_2 consumption was observed for $Co@SiO_2Al_2O_3$ OP catalyst. In addition, the lowest H_2 consumption was observed for $Co@SiO_2$ OP catalyst. This result suggests the presence of a greater number of reducible metal oxides in the $Co@SiO_2Al_2O_3$ OP catalyst. The H_2 consumption results are also supported by XRD analysis. In XRD analysis, no Co_3O_4 peaks are observed for the $Co@SiO_2$ OP catalyst. So, the H_2 consumption was less than that observed with other catalysts. The reduction degree of Co-based catalyst was calculated based on the literature [43]. The recommended temperature for the calculation of reduction degree

is 150–400 °C because the FT reaction occurred in this temperature range. The highest degree of reduction is observed for the $Co@SiO_2Al_2O_3$ OP catalyst, according to Table 4. The formation of the core–shell catalyst leads to an increase in reduction degree from 19.05 to 31.24%. With the addition of Al_2O_3 in the shell part, the reduction degree increases from 0.23 to 31.24% for one-pot synthesis catalyst. A similar trend is also observed in H_2 consumption. The increase in reduction degree leads to an increase in cobalt particle size which is found by other researchers [44, 45]. However, the cobalt oxide nanoparticle would be reduced easier to give cobalt active sites over the $Co@SiO_2Al_2O_3$ OP catalyst for FTS, which corresponds to a higher reduction degree among all core–shell catalysts.



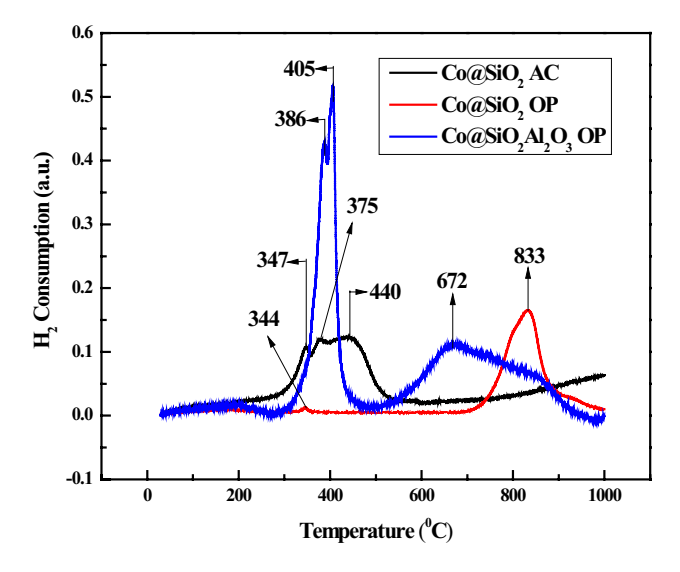


Fig. 6 H_2 -TPR profiles of all three Catalysts

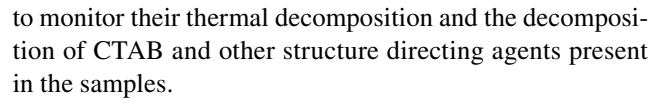
Table 4 H₂ Consumption of synthesized catalysts

Catalyst	H ₂ Consumption (mmol/g) ^a	Reduction degree (%) ^b
Co@SiO ₂ AC	0.42	19.05
Co@SiO ₂ OP	0.23	0.23
$Co@SiO_2Al_2O_3 OP$	0.91	31.24

^aThe H_2 consumption (mmol/g) was defined as the measured amount of H_2 consumption in TPR peak /theoretical H_2 consumption (mmol H_2 /g)×100

3.2.6 Thermo-Gravimetric Analysis and Differential Scanning Calorimetry (TGA–DSC)

Simultaneous thermo-gravimetric analysis (TGA) and differential scanning calorimetry (DSC) are the techniques to investigate the thermal characteristics of different substances. The decomposition temperature of polymer templates used in the mixed composite support preparation was determined by Thermo-gravimetry and Differential scanning Calorimetry (TGA–DSC). The samples were heated to 1000 °C at a heating rate of 10 °C/min. The analysis was done in the presence of airflow at 100 ml/min [46]. In TGA analysis, the sample is heated in the presence of airflow with a constant heat rate, and the difference in mass during this process is measured. In DSC analysis, critical thermal conditions like melting point and glass transition temperature of a substance can be obtained. As-synthesized (not calcined) samples were subjected to simultaneous TGA–DSC studies



In Fig. 7 for the case of Co@SiO₂ AC, the black line is weight loss, and the starting point is water, the second peak is CTAB which is a surfactant, and the third peak is due to PVP, which is the capping agent. The blue line indicates heat flow, and above 400 °C, everything is removed, and it continues to be very stable; it has 40% total weight loss. The first blue sharp peak corresponds to weight loss due to CTAB; the second sharp peak corresponds to that of PVP.

In Fig. 7b of Co@SiO₂ OP, two sharp peaks appear for heat flow, and they are due to exothermic reactions. In Fig. 7a, the weight loss peak is much smoother than Co@SiO₂ AC; it has a 60% total weight loss [47]. Figure 7c in the case of Co@SiO₂Al₂O₃ OP, the first weight loss below 175 °C is due to the removal of volatile solvents used for the catalyst preparation and water/moisture adsorbed on the support surfaces. The second weight loss between 175 °C and 245 °C was caused by the decomposition of the PVP template used for synthesis. The third weight loss from 255 °C to 360 °C corresponds to the decomposition of the surfactant CTAB, and it shows a 65% total weight loss [35, 43].

3.2.7 Fourier Transform Infrared Spectroscopy (FTIR)

The IR spectra of as-synthesized samples are shown in Fig. 8. The FTIR of the Co₃O₄ nanoparticle shows a band at 557 cm⁻¹, which is due to the (Co–O) mode [48]. The band at 1633 cm⁻¹ corresponds to the stretching and bending modes of the surface hydroxyls [49]. The IR spectrum of nanocomposite exhibits adsorptions at 1091 cm⁻¹, which is depicted as Si–O vibrations. The bands at 2844 and 2927 cm⁻¹ are basically for asymmetric and symmetric C-H stretching of the organics that disappeared after calcination [50]. The absorption of the Co–O vibrations decreased due to the presence of mesoporous SiO₂. There are no characteristic absorptions of Co–O-Si species; it suggests no chemical interaction between the Co₃O₄ core and SiO₂ shell [51].

3.2.8 XPS analysis

The oxidation states of the Co-active sites, as well as the differences in binding energy as a function of the Co support interactions, were investigated by deconvoluted XPS spectra analysis shown in Fig. 9. The conspicuous satellite peaks of Co^{2+} and Co^{3+} confirmed the presence of CoO and Co_3O_4 mixed oxides in all the supports suggesting that both oxidation states were involved in the FT reactions [52]. A close examination of each spectrum shows appreciable binding energy (peak) shifts that are distinctive from one catalyst to another. For example, the binding energy of the Co_2P of Co_3O_4 oxide for Co_2Si_2 AC extends to about



^bThe degree of reduction (%) was defined according to the literature [33] as the measured amount of H_2 consumption between 150–400 °C in TPR peak /theoretical H_2 consumption (mmol H_2/g)×100

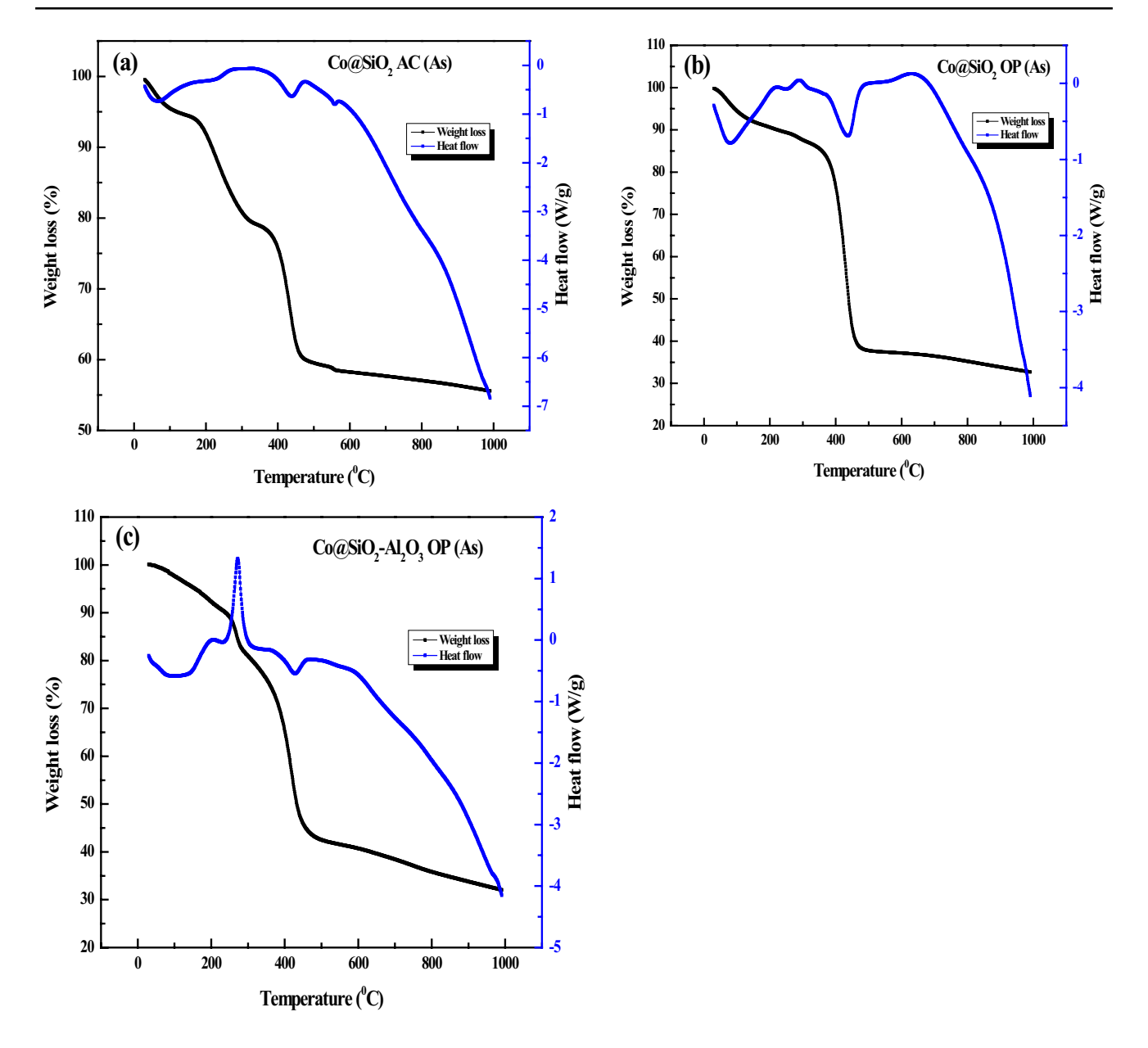


Fig. 7 TGA-DSC thermograms of a Co@SiO₂ AC (As); b Co@SiO₂ OP (As); c Co@SiO₂Al₂O₃ OP (As) catalysts

780.84 eV. However, when Aluminum oxide is added (i.e., Co@SiO₂Al₂O₃ OP), the binding energy of the Co2p spectra shifts a little further to 782.07 eV [53]. Also, about a 0.54 eV difference in the peak shift is noticed between the Co@SiO₂ AC and Co@SiO₂ OP catalysts. These differences and shifts in binding energy could be attributed to the fact that Co active sites interacted differently with each support, possibly due to the crystallinity differences of the support/material, which resulted from the different synthesis methods. [See supplemental Data] This observation is consistent with our crystallinity calculations in Sect. 3.2.2.

3.2.9 Fischer–Tropsch Synthesis (FTS) of Co-Based Core– Shell Catalysts

The effect of reaction temperature on different Co-based core–shell catalysts was studied to know the optimum reaction temperature for CO conversion and hydrocarbon selectivity. The reaction temperature was varied from 200 to 350 $^{\circ}$ C with a constant H₂:CO molar ratio (2:1), using 12,000 GHSV and 20 bar pressure. The N₂ gas flow rate was maintained at 1.5 ml/min.

CO conversion and hydrocarbon selectivity were calculated based on the following equations [48, 49].



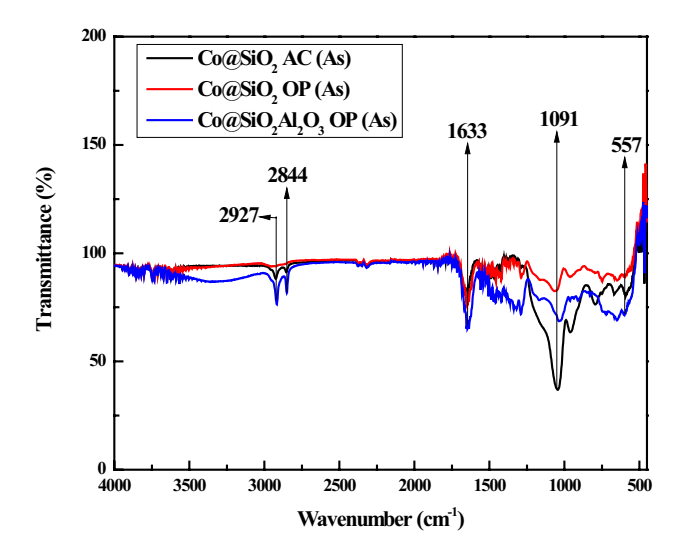


Fig. 8 FTIR analyses of all catalysts prior to calcination: **a** Co@SiO₂ AC (As); **b** Co@SiO₂ OP(As); **c** Co@SiO₂Al₂O₃ OP(As) Catalyst

$$X_{CO}\% = \frac{F_{CO,in} - F_{CO,out}}{F_{CO.in}} \times 100$$

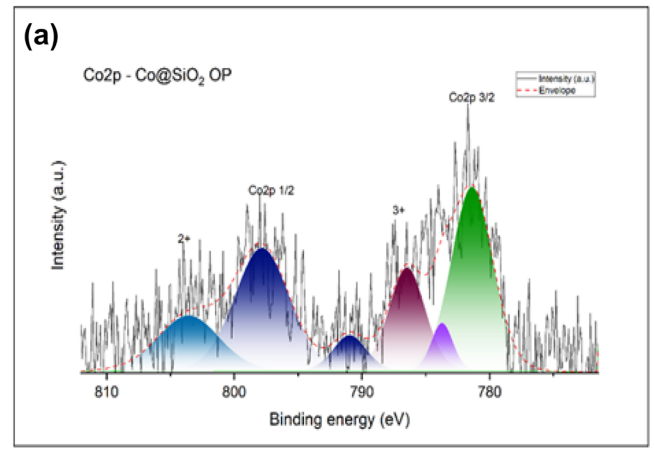
$${\rm CH_4Selectivity}~(\%~) = \frac{mCH_4}{mCH_4 + 2mC_2H_6 + 3mC_3H_8 + 4mC_4H_{10}} \times 100$$

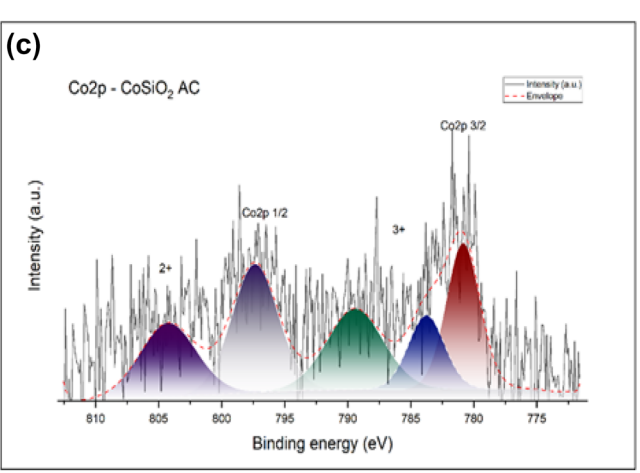
$$C_2H_6$$
Selectivity (%) = $\frac{2mC_2H_6}{mCH_4 + 2mC_2H_6 + 3mC_3H_8} \times 100$

$$C_3H_8$$
Selectivity (%) = $\frac{3mC_3H_8}{mCH_4 + 2mC_2H_6 + 3mC_3H_8} \times 100$

Although the production of CO₂ from the water gas shift reaction is important,

Figure 10 shows the effect of reaction temperature on CO conversion and product selectivity for $Co@SiO_2$ AC catalyst. CO conversion increases with the increase in temperature up to 350 °C, then show a declining trend at elevated temperatures. This was probably due to a reverse water–gas





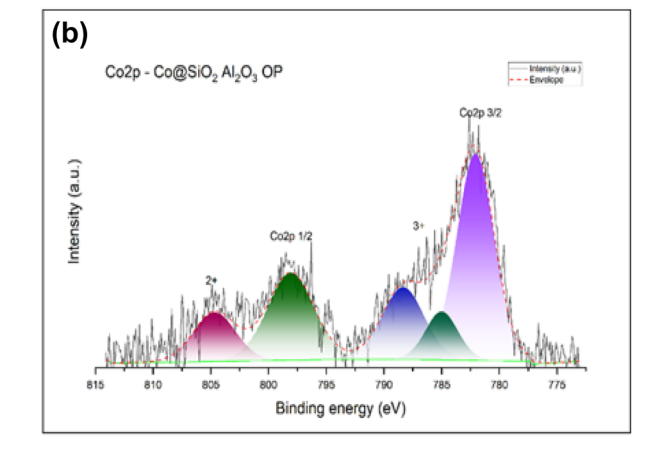


Fig. 9 XPS Spectra of: a Co@SiO $_2$ OP b Co@SiO $_2$ Al $_2$ O $_3$ OP c Co@SiO $_2$ AC



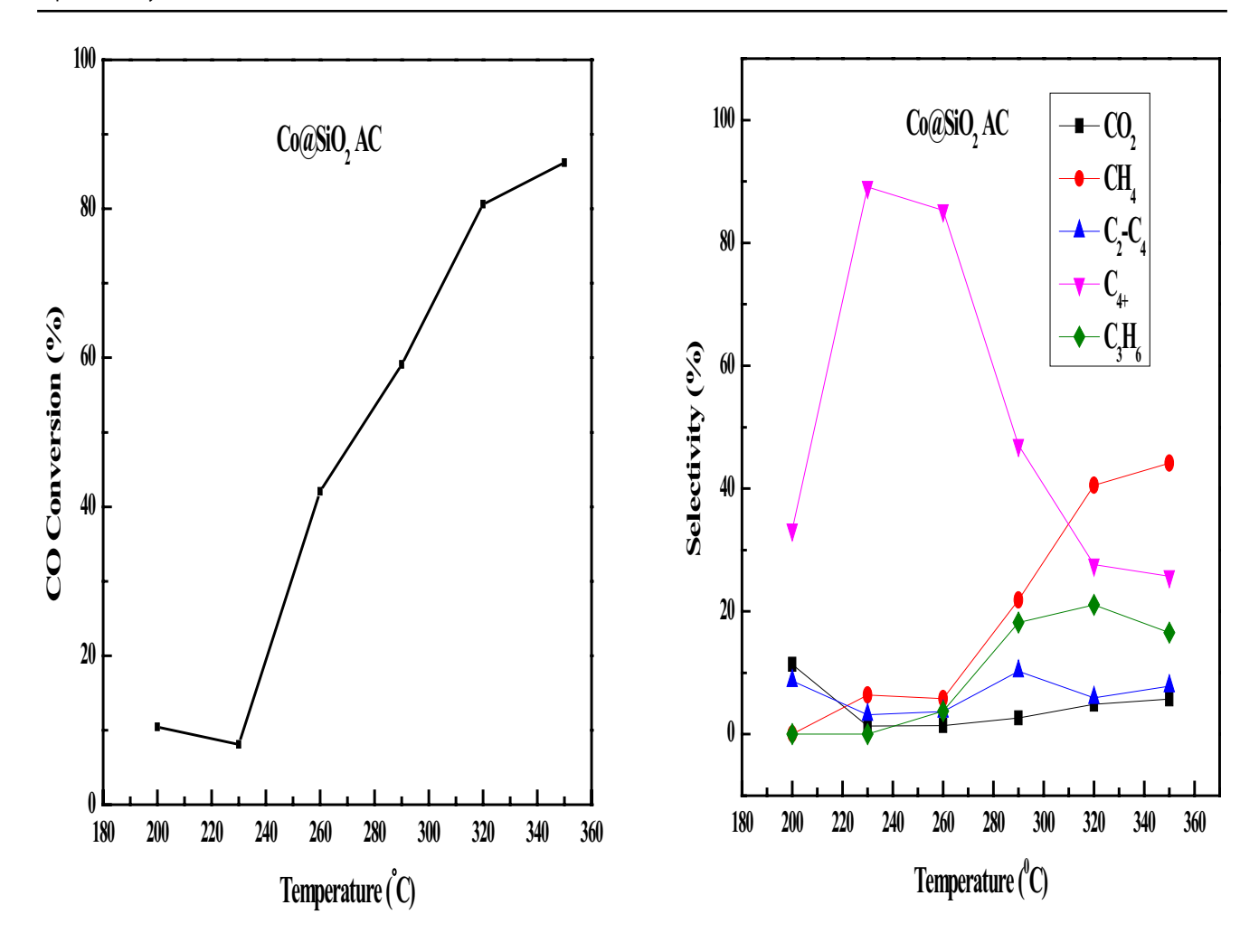


Fig. 10 Effect of temperature on CO conversion and product selectivity in FT synthesis using $Co@SiO_2$ AC catalyst (Conditions: $H_2/CO = 2$, 20 bar, 12,000 GHSV, and $N_2 = 1.5$ ml/min)

shift reaction, which occurred at a higher temperature. The C_2 – C_4 selectivity was almost unchanged throughout the temperature range. The methane selectivity increased with the increase of reaction temperature. In addition, light olefin (C_3H_6) was produced in this temperature range. C_3H_6 selectivity increased with the increase in temperature. and the higher hydrocarbon (C_{4+}) selectivity decreased at a higher temperature.

In Fig. 11, CO@ $SiO_2Al_2O_3$ OP catalyst activity was studied by variation of reaction temperature with other fixed reaction parameters ($H_2/CO=2$, 20 bar, 12,000 GHSV, and $N_2=1.5$ ml/min). CO conversion increased throughout the temperature range. CO conversion was almost stable between 300 to 325 °C. After that, it increased again up to 350 °C. The highest CO conversion was obtained at 350 °C. Methane selectivity increased, and consequently, the higher hydrocarbon selectivity (C_{4+}) decreased from 260 to 350 °C. C_2 – C_4 hydrocarbon selectivity was almost constant throughout this temperature range.

Figure 12 shows the $Co@SiO_2$ OP catalyst activity in terms of CO conversion and product selectivity with the variation of reaction temperature. The CO selectivity increased with the increase in temperature. CH_4 selectivity increased a little at a higher temperature. However, higher hydrocarbon selectivity was observed when it is compared to other catalysts in this temperature range. C_2 – C_4 selectivity was almost constant with the increase in temperature.

The water gas shift reaction is exothermic, and the FT reaction is thermodynamically favorable for the conversion of CO_2 in the presence of H_2 to form CO at high temperatures [10].

Figure 13 shows how the CO conversion is affected by temperature for Co@SiO₂ OP. While the conversion is quite low, about 5% at 200 °C, it increased steadily and reached a maximum at 350 °C. The CO conversion increased by 15%. Conversely, our findings elucidated that the addition of metal promoters to the Co@SiO₂ play distinctive and significant



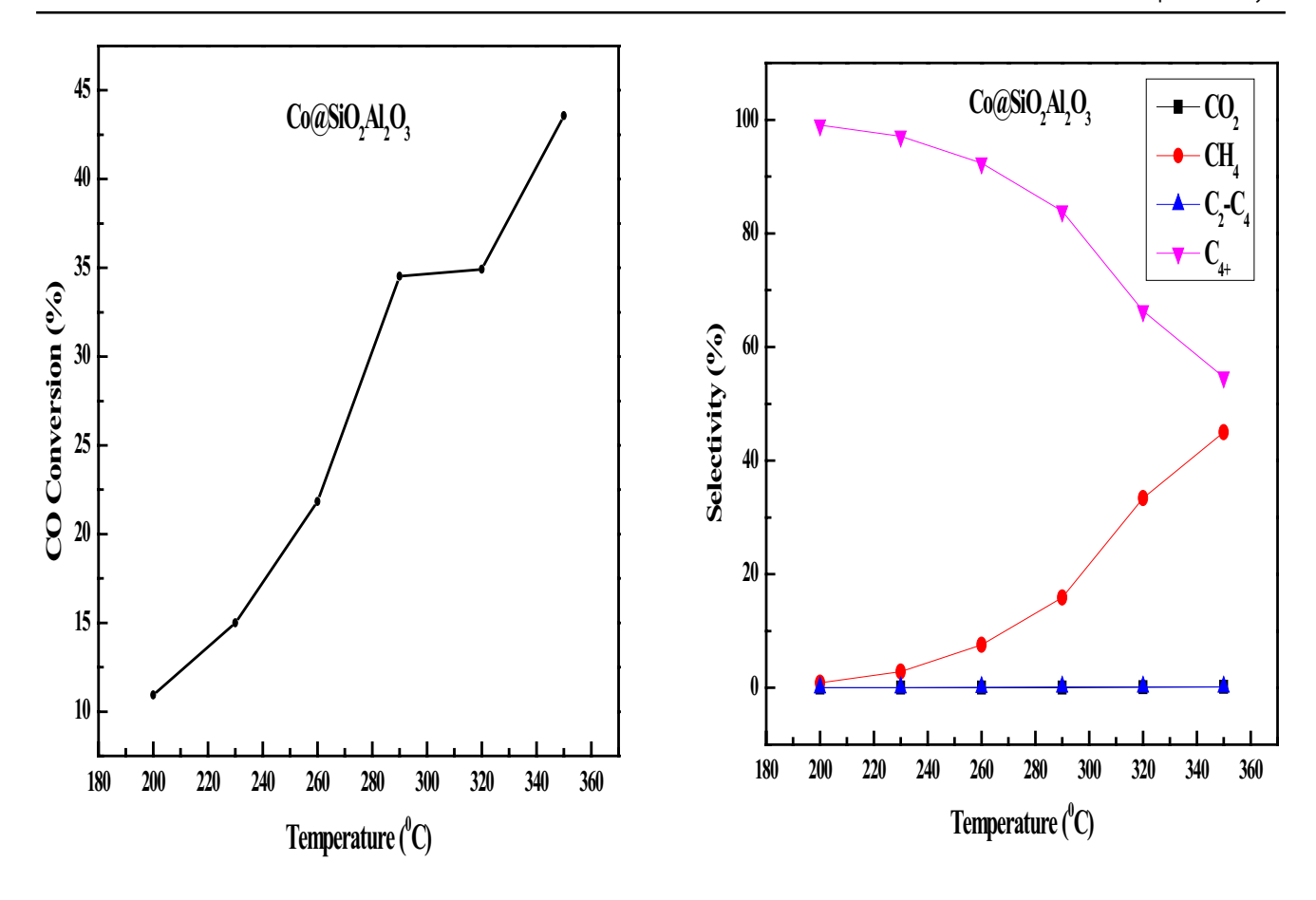


Fig. 11 Effect of temperature on CO conversion and product selectivity in FT synthesis using $Co@SiO_2Al_2O_3$ OP catalyst (Conditions: $H_2/CO=2$, 20 bar, 12,000 GHSV, and $N_2=1.5$ ml/min)

roles in the syngas conversion and C₁–C₄ product distribution at 20 bar.

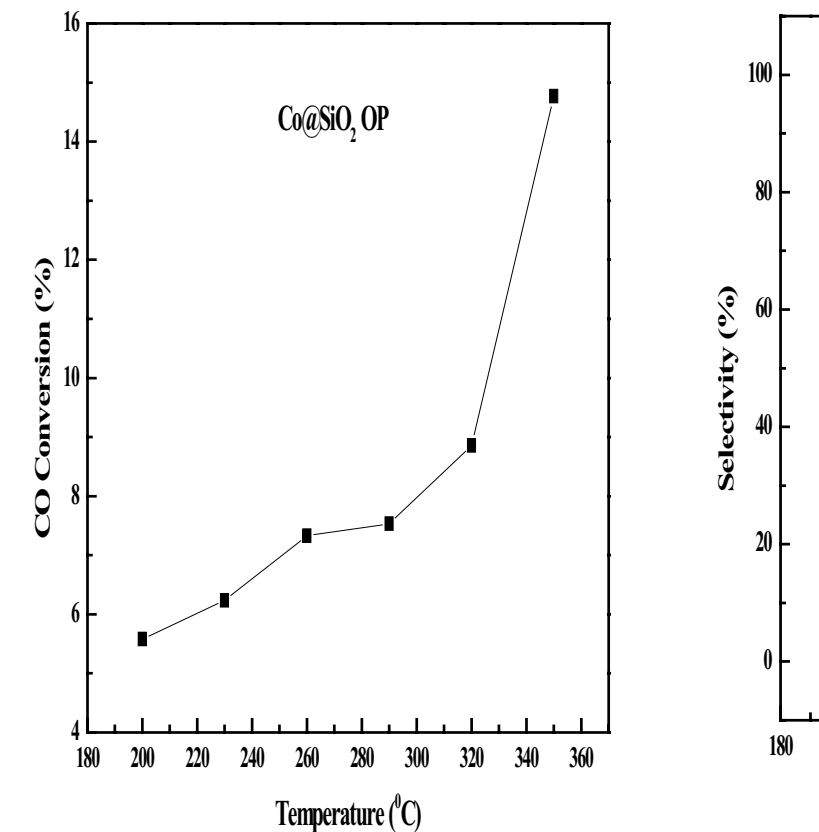
When two one-pot synthesis catalysts are compared, Co@ $SiO_2Al_2O_3$ OP showed promising results in terms of CO conversion and hydrocarbon selectivity. Addition of Al_2O_3 in the shell part of the Co@SiO₂ catalyst increased the CO conversion from 15 to 45% at 350 °C. This suggests that the enhancement of reduction degree from 0.23% to 31.24% in which higher metallic Co sites were obtained for FTS. The main reason was the formation of core—shell structure leads to electronic interaction of core atoms on shell surface ones, which corresponded to higher catalytic activity for CO@ $SiO_2Al_2O_3$ OP catalyst [54].

3.3 Time-on-Stream Study of All Catalysts

To investigate the time-on-stream behavior of all catalysts, the FTS reaction was carried out for 50 h. In the case of the Co@SiO₂ AC catalyst, the almost stable CO conversion was

obtained for up to 30 h. Then the CO conversion decreased from 30 to 50 h. The stable conversion was obtained after 20 h for the Co@SiO₂ OP catalyst. The CO conversion increased a little from 20 to 35 h. After that, the conversion slightly decreased between 35 to 50 h of reaction. In the case of the Co@SiO₂Al₂O₃ OP catalyst, after an initial decrease of CO conversion up to 15 h, the CO conversion was almost stable between 15 and 25 h. The conversion further decreased sharply from 25 to 35 h. Then, it was stable from 35 to 45 h. After that, it decreased again up to 50 h. The decreasing trend of CO conversion suggests that the catalyst was deactivated due to coke deposition over the catalyst surface. The lower hydrocarbon selectivity was almost constant during the time-on-stream study for all catalysts. C₄₊ selectivity was initially higher and continuously decreased later for the Co@SiO₂Al₂O₃ OP catalyst. In the case of other catalysts, C₄₊ selectivity was almost constant during the timeon-stream study. However, the lighter olefin (C_3H_6) selectivity was almost constant throughout the stability study.





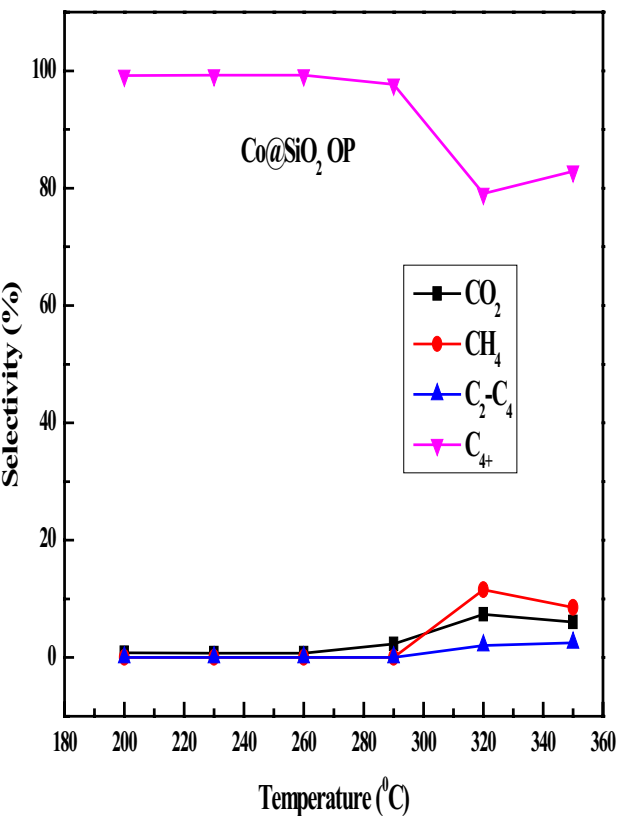


Fig. 12 Effect of temperature on CO conversion and product selectivity in FT synthesis using $Co@SiO_2$ OP catalyst (Conditions: $H_2/CO = 2$, 20 bar, 12,000 GHSV, and $N_2 = 1.5$ ml/min)

3.4 Spent Catalysts Characterization

3.4.1 XRD Analysis

Figure 14 shows the XRD analysis of the spent Co@SiO-2Al₂O₃ OP catalyst. It indicates the formation of an amorphous structure and the disappearance of the crystal structure. The peak intensity of metal oxides was reduced.

3.4.2 SEM Analysis

Figure 15 shows the SEM morphologies of spent catalysts. The surface morphology changed after the stability study. Particle agglomeration was observed in all spent catalysts. The formation of coke is visible over the catalyst surface during the Fischer–Tropsch synthesis in the microchannel microreactor. The coke formation is also one of the main contributions to the retardation of catalyst activity.

3.4.3 TGA-DSC Analyses

Figure 16 shows the TGA–DSC analysis of the spent catalysts. Almost 12 wt.% loss was observed during the analysis for Co@SiO₂ OP and Co@SiO₂Al₂O₃ OP catalysts. However, 40 wt.% weight loss was observed for Co@SiO₂ AC catalyst. This weight loss is attributed to the burning of coke in the presence of air during analysis. However, the coke deposition is the main factor for catalyst deactivation, but other factors (method of preparation, composition of mixed oxide support, oxidation, sintering, support degradation, and attrition) also affect catalyst deactivation. The high reducibility property of the Co@SiO₂Al₂O₃ catalyst (From TPR analysis) could be the factor for catalyst deactivation.



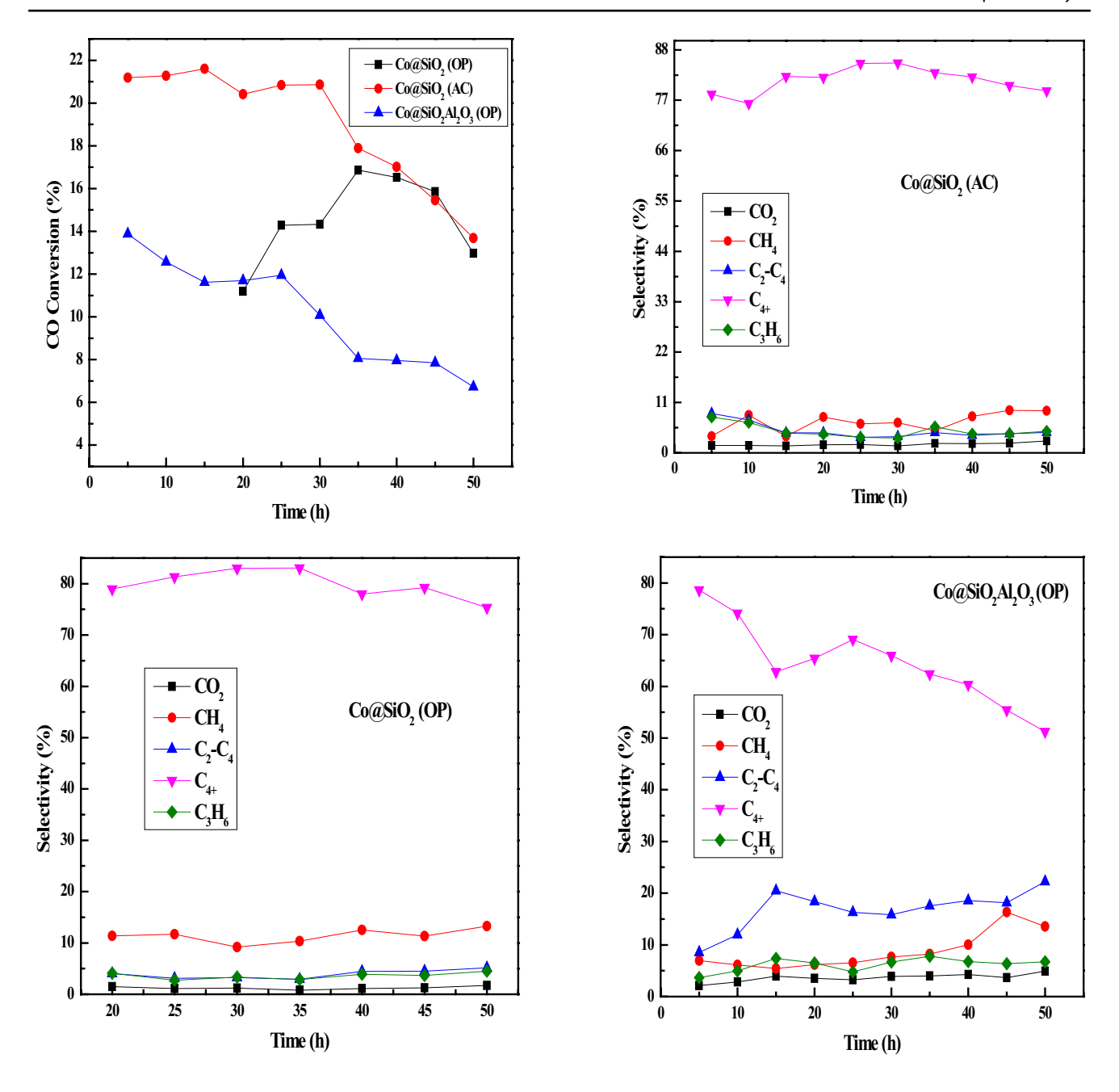


Fig. 13 Time-on-stream behavior of $Co@SiO_2$ AC, $Co@SiO_2$ OP and $Co@SiO_2Al_2O_3$ OP catalysts (Conditions: $H_2/CO=2$, 20 bar, 12,000 GHSV at 260. °C, $N_2=1.5$ ml/min)

4 Experimental Summary

In this work, a 3D printed stainless steel microchannel microreactor was used for FT synthesis to evaluate the catalyst performance of two different cobalt-based mesoporous oxides. Catalysts were prepared using autoclave and one-pot hydrothermal synthesis methods. The property of the

Co@SiO₂ (AC), Co@SiO₂ (OP), and Co@SiO₂Al₂O₃ (OP) catalysts was determined with the aid of using the N₂ physisorption technique. The catalysts showed N₂ adsorption–desorption isotherm and confirmed an average Type-IV isotherm with a protracted hysteresis loop and capillary condensation. BET surface area observed that the surface area, pore volume and average pore size certainly. XRD is



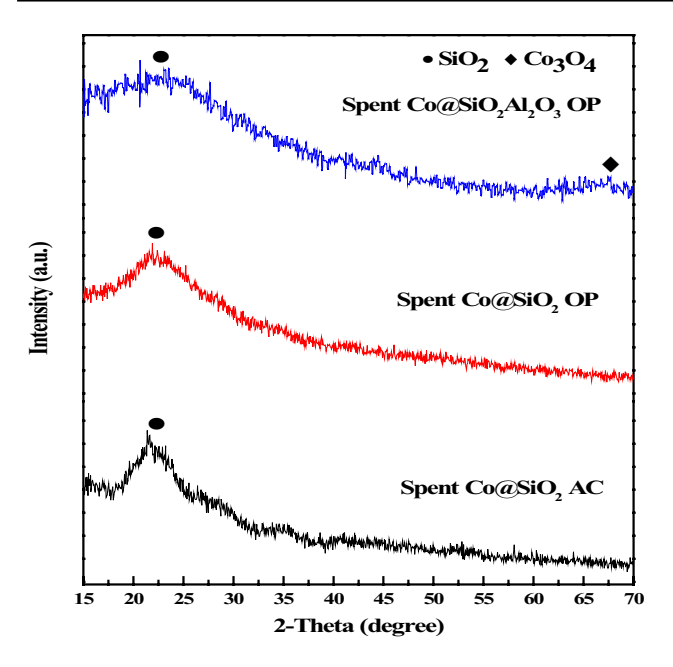


Fig. 14 XRD analysis of all Spent catalysts

used for the primary characterization of material properties like crystal structure and crystallite size. The mesoporous nature is indicated by $\rm N_2$ adsorption Type IV isotherms. To recognize the crystal shape, a wide-angle XRD evaluation was performed. The SEM images had been used for the morphology and composition of every catalyst. Silica is usually used in core—shell catalysts due to its mechanical strength, structural traits, and smoothness for surface functionalization. The particles are properly dispersed for the $\rm Co@SiO_2$ (AC) and $\rm Co@SiO_2$ (OP) catalysts. The SEM characterization also indicated the presence of agglomerates in the $\rm Co@SiO_2Al_2O_3$ (OP) catalyst due to the incorporation of $\rm Al_2O_3$ into the mesoporous silica shell.

The size of cobalt particles and the thickness of the silica layer are both different for different synthesis methods. It has been reported by other groups that the silica layer suppresses the growth of cobalt particles [6]. When two methods are compared, autoclave synthesis is much better as one-pot synthesis produces agglomeration of particles. TPR analysis was performed to study the reduction behavior of the metal oxide catalysts and evaluate the metal-support interaction. TPR result shows that the synthesis method plays an important role in the reduction of metal oxide. The results from TPR studies are supported by TEM analysis.

As-synthesized samples were subjected to simultaneous TGA-DSC studies to monitor their thermal decomposition. Co@SiO₂ OP, during heat flow, two sharp peaks appear, these peaks are gone out, and it is an exothermic reaction.

The weight loss peak is much smoother than Co@SiO₂ AC; it has a 60% total weight loss. Co@SiO₂Al₂O₃ OP weight loss due to the removal of volatile solvents used for the catalyst preparation and water/moisture adsorbed on the support surfaces. The selectivity toward methane reduced with growth inside the temperature, after which multiplied sharply on the rate of longer chain hydrocarbons at expanded temperatures for all of the catalysts.

Three different catalysts were tested for FT-SSMR activity studies. The effect of temperature (200-390 °C) on CO conversion and selectivity of CO₂, CH₄, C₂H₆, C₃H₈, C₄H₁₀, and C_{4+} products are reported in Figs. 9, 10, 11, 12, 13, 14, 15. Preliminary FT-SSMR reactions were performed with all catalysts; based on each catalyst's ability to CO conversion, stability, and hydrocarbon selectivity [8]. In general, low CO conversion is accompanied by low temperature, and high CO conversion is accompanied by high temperature. Higher CO conversion was obtained for the Co@SiO₂ AC catalyst, 85% at 350 °C, as shown in Fig. 11. The highest selectivity was obtained Co@SiO₂Al₂O₃ OP catalyst, 99% at 200 °C in Fig. 12. High temperature (300-350 °C) FT (HTFT) activity revealed that the Co@SiO₂Al₂O₃ OP catalyst showed the highest hydrocarbon selectivity. Particularly at 200 °C, C₄₊ hydrocarbon selectivity was as high as 99%, while methane selectivity at 350 °C was approximately 45%. This confirmed the well-known suitability of Co catalysts for FT activity.

Catalysts	CO Conver- sion %
Co@SiO ₂ AC SS Microreactors	85%
Co@SiO ₂ Al ₂ O ₃ OP SS Microreactors	45%
Co@SiO ₂ OP SS Microreactors	27%

5 Conclusion

The Core–Shell catalysts were successfully synthesized using the autoclave and one-pot synthesis techniques and resulted in a high surface area Co@SiO₂ matrix with an ordered mesoporous structure as supported by XRD and BET surface area studies. TEM and SEM–EDX results indicate a clear hexagonal matrix having porous surface morphology with uniform metal ion distribution. The stainless steel microreactors fabricated by 3D-printing technology were successfully used to study the effect of core–shell catalysts in FT synthesis at 20 bar [55].

For FT synthesis with operating conditions of 20 bar, H_2 : CO (2:1), and the temperature range 200–370 °C, all



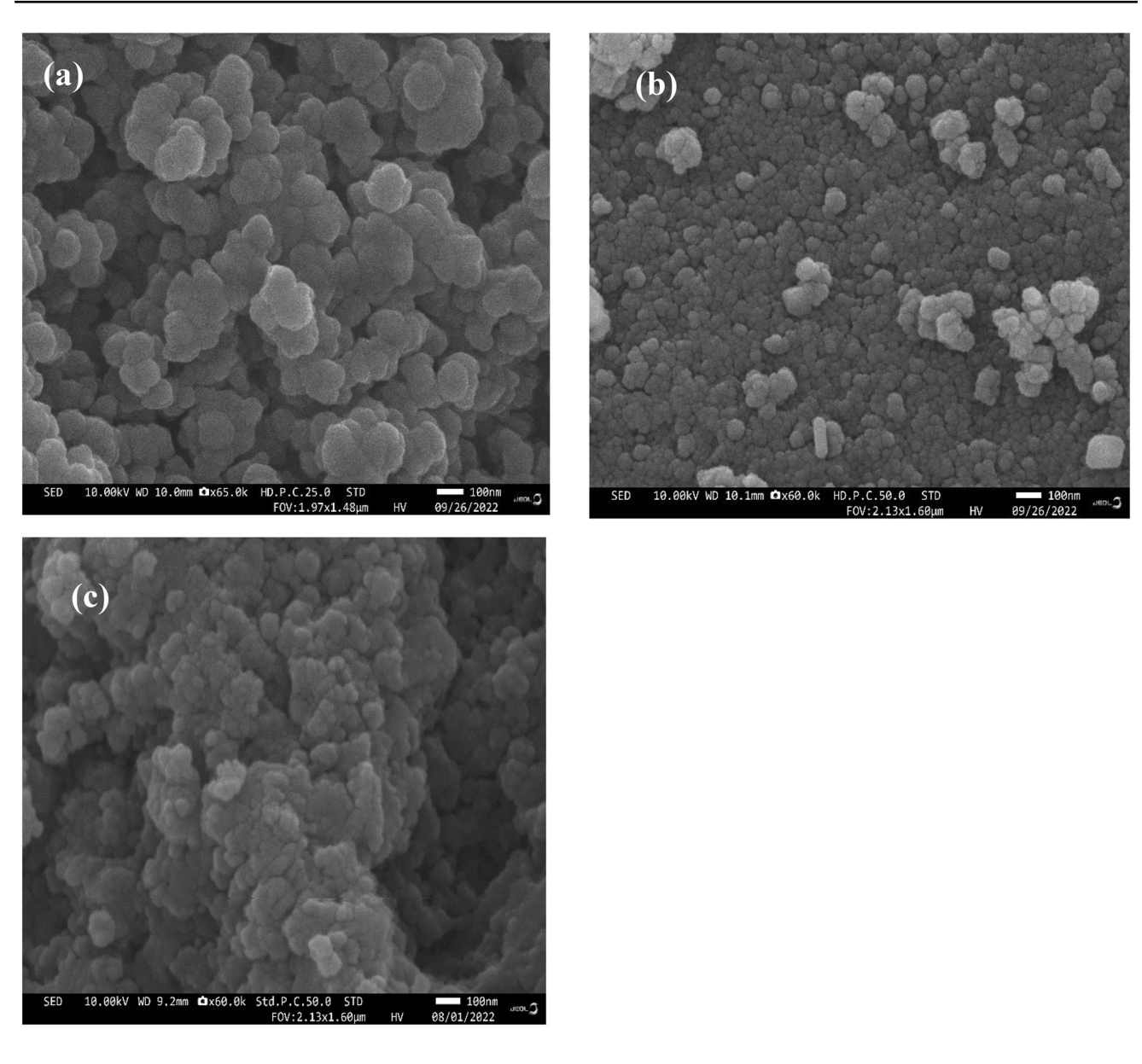


Fig. 15 SEM images of Spent a Co@SiO₂ AC; b Co@SiO₂ OP; c Co@SiO₂Al₂O₃ OP catalysts

the catalysts showed similar trends in CO conversion. The highest CO conversion for $Co@SiO_2$ AC (85%), $Co@SiO_2Al_2O_3$ OP (45%), and 27% for the $Co@SiO_2$ OP catalyst. With regard to the % selectivity of $Co@SiO_2$ AC in SS Microreactors, C_{4+} is the highest in the temperature range of 200-300 °C and follows the order: $Co@SiO_2AC > Co@SiO_2Al_2O_3$ OP > $Co@SiO_2$ OP FT SS Microreactors.

Among all the catalysts studied, Co@SiO₂ AC showed the strongest resistance to deactivation. This study suggests that the addition of another transition metal to Co-SiO₂ can play

a vital role in FT synthesis. Finally, the 3D-printed stainless steel microreactor enables ease of catalyst screening and development, addressing major issues with Fischer–Tropsch Synthesis.

Supplementary Information The online version contains supplementary material available at https://doi.org/10.1007/s11244-022-01733-z.

Acknowledgements The authors gratefully acknowledge the help from Dr. Kyle Nowlin for TEM studies at Joint School of Nanoscience and Nanoengineering, Dr. Shima Masoumi and Dr. Xin Li for SEM and XRD studies, Mr. Saif Hassan for TGA-DSC analyses, and Mr. Xiao Ma and Ms. Nourigheimasi Farnoush for XRD studies at Wake Forest University.



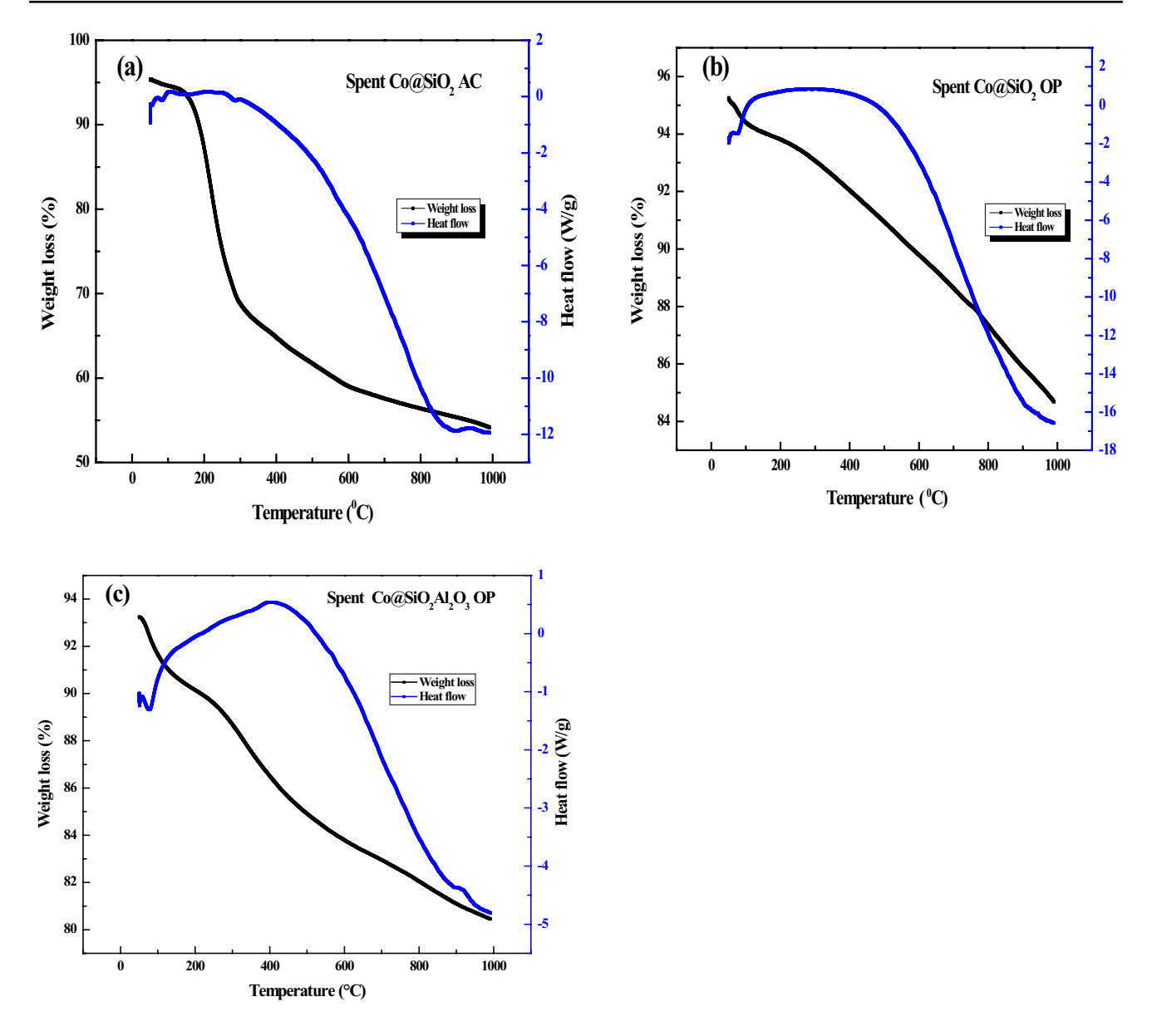


Fig. 16 TGA–DSC analyses of Spent a Co@SiO₂ AC; b Co@SiO₂ OP; c Co@SiO₂Al₂O₃ OP catalysts

Funding This work was performed at North Carolina A&T State University, the Department of Applied Science Technology, the Department of Chemistry, and the Joint School of Nanoscience and Nanoengineering, a member of Southeastern Nanotechnology Infrastructure Corridor (SENIC) supported by National Science Foundation, USA (Grant ECCS-1542174). This project was partially supported by funds provided by National Science Foundation-Center of Research Excellence in Science and Technology, USA (HRD #1736173) and the University of North Carolina System-Research Opportunities Initiative(UNC-ROI 2017).

References

 Panda A, Kim E, Choi YN et al (2019) Phase controlled synthesis of Pt doped co nanoparticle composites using a metal-organic

- framework for Fischer–Tropsch catalysis. Catalysts 9:156. https://doi.org/10.3390/CATAL9020156
- DE484337C—Process for the catalytic production of multi-membered paraffinic hydrocarbons from carbon oxides and hydrogen

 Google Patents. https://patents.google.com/patent/DE484337C/en. Accessed 5 Aug 2022
- Steynberg AP (2004) Chapter 1—introduction to Fischer-Tropsch technology. In: Steynberg A et al (eds) Fischer-Tropsch technology. Elsevier, pp 1–63
- Jager B, Espinoza R (1995) Advances in low temperature Fischer-Tropsch synthesis. Catal Today 23:17–28. https://doi.org/10.1016/ 0920-5861(94)00136-P
- Sie ST (1998) Process development and scale up: IV. Case history
 of the development of a fischer-tropsch synthesis process. Rev
 Chem Eng 14:109–157. https://doi.org/10.1515/REVCE.1998.
 14.2.109/MACHINEREADABLECITATION/RIS



- Bepari S, Stevens-Boyd R, Mohammad N et al (2021) Composite mesoporous SiO2-Al2O3 supported Fe, FeCo and FeRu catalysts for Fischer-Tropsch studies in a 3-D printed stainless-steel microreactor. Mater Today Proc 35:221–228. https://doi.org/10.1016/J. MATPR.2020.04.582
- Mohammad N, Abrokwah RY, Stevens-Boyd RG et al (2020) Fischer-Tropsch studies in a 3D-printed stainless steel microchannel microreactor coated with cobalt-based bimetallic-MCM-41 catalysts. Catal Today 358:303–315. https://doi.org/10.1016/J.CATTOD.2020.02.020
- Bepari S, Li X, Abrokwah R et al (2020) Co-Ru catalysts with different composite oxide supports for Fischer-Tropsch studies in 3D-printed stainless steel microreactors. Appl Catal A Gen. https://doi.org/10.1016/j.apcata.2020.117838
- Mohammad N, Kuila D, Aravamudhan S (2020) Catalyst and microreactor development for atmospheric and high-pressure Fischer-Tropsch synthesis. North Carolina Agricultural and Technical State University
- Mohammad N, Basha OM, Bepari S et al (2021) Fischer-Tropsch synthesis in silicon and 3d printed stainless steel microchannel microreactors. Catal Clean Energy Environ Sustain. https://doi. org/10.1007/978-3-030-65021-6_14
- Cybulski A, Edvinsson R, Irandoust S, Andersson B (1993) Liquid-phase methanol synthesis: modelling of a monolithic reactor. Chem Eng Sci 48:3463–3478. https://doi.org/10.1016/0009-2509(93)85002-7
- Davis BH (2002) Overview of reactors for liquid phase Fischer-Tropsch synthesis. Catal Today 71:249–300. https://doi.org/10. 1016/S0920-5861(01)00455-2
- Mohammad N, Bepari S, Aravamudhan S, Kuila D (2019) Kinetics of Fischer-Tropsch synthesis in a 3-D printed stainless steel microreactor using different mesoporous silica supported Co-Ru catalysts. Catalysts 9:872. https://doi.org/10.3390/CATAL91008
- Das D, Samal DP, Mohammad N, Meikap BC (2017) Hydrodynamics of a multi-stage counter-current fluidized bed reactor with down-comer for amine impregnated activated carbon particle system. Adv Powder Technol 28:854

 –864. https://doi.org/10.1016/J. APT.2016.12.011
- Jager B (1997) Developments in Fischer-Tropsch technology. Stud Surf Sci Catal 107:219–224. https://doi.org/10.1016/S0167-2991(97)80338-2
- Mohammad N, Chukwudoro C, Bepari S et al (2022) Scale-up of high-pressure F-T synthesis in 3D printed stainless steel microchannel microreactors: Experiments and modeling. Catal Today 397–399:182–196. https://doi.org/10.1016/J.CATTOD.2021.09. 038
- Schulz H (1999) Short history and present trends of Fischer-Tropsch synthesis. Appl Catal A Gen 186:3–12. https://doi.org/ 10.1016/S0926-860X(99)00160-X
- Singleton AH (1997) Advances make gas-to-liquids process competitive for remote locations. Oil Gas J 95
- Eisenberg B, Fiato RA, Mauldin CH et al (1998) Exxons advanced gas-to-liquids technology. Elsevier
- Davis BH (1997) Fischer-Tropsch conversion of gas to liquid.
 Appl Catal A Gen 155:N4–N7. https://doi.org/10.1016/S0926-860X(97)80024-5
- Geng S, Mao ZS, Huang Q, Yang C (2021) Process intensification in pneumatically agitated slurry reactors. Engineering 7:304

 –325. https://doi.org/10.1016/J.ENG.2021.03.002
- Deshmane VG, Abrokwah RY, Kuila D (2015) Synthesis of stable Cu-MCM-41 nanocatalysts for H2 production with high selectivity via steam reforming of methanol. Int J Hydrogen Energy 40:10439–10452. https://doi.org/10.1016/j.ijhydene.2015.06.084

- Rouquerol F, Rouquerol J, Sing K et al (1999) Chapter 1—introduction. Adsorption by powders and porous solids. Elsevier, pp 1–26
- García Blanco AA, Gabriela Amaya M, Eugenia Roca Jalil M et al (2011) Effect of the synthesis method on co-catalysts based on MCM-41 for the Fischer-Tropsch reaction. Top Catal. https:// doi.org/10.1007/s11244-011-9638-5
- Ni Z, Kang S, Bai J et al (2017) Uniformity dispersive, anti-coking core@double-shell-structured Co@SiO2@C: effect of graphitic carbon modified interior pore-walls on C5+ selectivity in Fischer-Tropsch synthesis. J Colloid Interface Sci 505:325–331. https:// doi.org/10.1016/J.JCIS.2017.05.096
- González O, Pérez H, Navarro P et al (2009) Use of different mesostructured materials based on silica as cobalt supports for the Fischer-Tropsch synthesis. Catal Today 148:140–147. https:// doi.org/10.1016/J.CATTOD.2009.03.030
- Xie R, Wang H, Gao P et al (2015) Core@shell Co3O4@C-m-SiO2 catalysts with inert C modified mesoporous channel for desired middle distillate. Appl Catal A Gen 492:93–99. https://doi.org/10.1016/J.APCATA.2014.12.023
- Bartholomew CH (2001) Mechanisms of catalyst deactivation.
 Appl Catal A Gen 212:17–60. https://doi.org/10.1016/S0926-860X(00)00843-7
- Dry ME (1991) (1990) Fischer-Tropsch synthesis over iron catalysts. Catal Lett 71(7):241–251. https://doi.org/10.1007/BF00764506
- Bartholomewa CH, Stoker MV, Manskerb L, Datyeb A (1999)
 Effects of pretreatment, reaction, and promoter on microphase structure and Fischer-Tropsch activity of precipitated iron catalysts. Elsevier
- Ernst B, Libs S, Chaumette P, Kiennemann A (1999) Preparation and characterization of Fischer-Tropsch active Co/SiO2 catalysts. Appl Catal A Gen 186:145–168. https://doi.org/10.1016/S0926-860X(99)00170-2
- Saleh TA (2015) Nanocomposite of carbon nanotubes/silica nanoparticles and their use for adsorption of Pb(II): from surface properties to sorption mechanism. New Pub Balaban 57:10730–10744. https://doi.org/10.1080/19443994.2015.1036784
- Monshi A, Foroughi MR, Monshi MR et al (2012) Modified Scherrer equation to estimate more accurately nano-crystallite size using XRD. World J Nano Sci Eng 2:154–160. https://doi. org/10.4236/WJNSE.2012.23020
- Rotaru R, Savin M, Tudorachi N et al (2017) Ferromagnetic iron oxide-cellulose nanocomposites prepared by ultrasonication. Polym Chem. https://doi.org/10.1039/C7PY01587A
- Chu W, Chernavskii PA, Gengembre L et al (2007) Cobalt species in promoted cobalt alumina-supported Fischer-Tropsch catalysts. J Catal 252:215–230. https://doi.org/10.1016/J.JCAT.2007.09.018
- Saleh TA (2015) Isotherm, kinetic, and thermodynamic studies on Hg(II) adsorption from aqueous solution by silica- multiwall carbon nanotubes. Environ Sci Pollut Res 22:16721–16731. https:// doi.org/10.1007/S11356-015-4866-Z/FIGURES/13
- Saleh TA (2015) Mercury sorption by silica/carbon nanotubes and silica/activated carbon: a comparison study. J Water Supply Res Technol 64:892–903. https://doi.org/10.2166/AQUA.2015.050
- 38. Lv X, Yuan S, Zhang Y et al (2019) Preparation of cyclonic Co3O4/Au/mesoporous SiO2 catalysts with core–shell structure for solvent-free oxidation of benzyl alcohol. J Taiwan Inst Chem Eng 102:448–455. https://doi.org/10.1016/J.JTICE.2019.06.013
- Li F, Wang M, Zhang J et al (2022) Sandwich-type Co core@ shell nanocomposite (SiO2 @Co@CeO2): coke resistant catalyst toward CO2 reforming with ethanol. Appl Catal A Gen 638:118605. https://doi.org/10.1016/J.APCATA.2022.118605
- Mirzaei F, Rezaei M, Meshkani F, Fattah Z (2015) Carbon dioxide reforming of methane for syngas production over Co–MgO mixed



- oxide nanocatalysts. J Ind Eng Chem 21:662–667. https://doi.org/10.1016/J.JIEC.2014.03.034
- Cho JH, Park JH, Chang TS et al (2012) Reductive amination of 2-propanol to monoisopropylamine over Co/γ-Al2O3 catalysts. Appl Catal A Gen 417–418:313–319. https://doi.org/10.1016/J. APCATA.2012.01.011
- Rosynek MP, Polansky CA (1991) Effect of cobalt source on the reduction properties of silica-supported cobalt catalysts. Appl Catal 73:97–112. https://doi.org/10.1016/0166-9834(91)85115-C
- Li YP, Wang TJ, Wu CZ et al (2009) Effect of Ru addition to Co/ SiO2/HZSM-5 catalysts on Fischer-Tropsch synthesis of gasolinerange hydrocarbons. Catal Commun 10:1868–1874. https://doi. org/10.1016/J.CATCOM.2009.06.021
- Trépanier M, Dalai AK, Abatzoglou N (2010) Synthesis of CNTsupported cobalt nanoparticle catalysts using a microemulsion technique: role of nanoparticle size on reducibility, activity and selectivity in Fischer-Tropsch reactions. Appl Catal A Gen 374:79–86. https://doi.org/10.1016/J.APCATA.2009.11.029
- Park JY, Lee YJ, Karandikar PR et al (2012) Fischer-Tropsch catalysts deposited with size-controlled Co3O4 nanocrystals: Effect of Co particle size on catalytic activity and stability. Appl Catal A Gen 411–412:15–23. https://doi.org/10.1016/J.APCATA.2011. 10.010
- Laboureur D, Glabeke G (2019) Gouriet JB (2019) Aluminum nanoparticles oxidation by TGA/DSC. J Therm Anal Calorim 1374(137):1199–1210. https://doi.org/10.1007/S10973-019-08058-2
- Gill P, Moghadam TT, Ranjbar B (2010) Differential scanning calorimetry techniques: applications in biology and nanoscience. J Biomol Tech 21:167
- Pejova B, Isahi A, Najdoski M, Grozdanov I (2001) Fabrication and characterization of nanocrystalline cobalt oxide thin films. Mater Res Bull 36:161–170. https://doi.org/10.1016/S0025-5408(00)00479-7
- He T, Chen D, Jiao X (2004) Controlled synthesis of Co3O4 nanoparticles through oriented aggregation. Chem Mater 16:737–743.

- https://doi.org/10.1021/CM0303033/SUPPL_FILE/CM0303033_S.PDF
- Meng Y, Chen D, Jiao X (2006) Fabrication and characterization of mesoporous Co3O4 core/mesoporous silica shell nanocomposites. J Phys Chem B 110:15212–15217. https://doi.org/10.1021/ JP0626465/SUPPL FILE/JP0626465SI20060618 045155.PDF
- Ocana M, Gonzalez-Elipe AR (1999) Preparation and characterization of uniform spherical silica particles coated with Ni and Co compounds. Colloids Surfaces A Physicochem Eng Asp 157:315–324. https://doi.org/10.1016/S0927-7757(99)00088-6
- Gao Z, Zhao D, Cheng Q et al (2021) Mesoporous SiO2-encapsulated nano-Co3O4 catalyst for efficient CO oxidation. Chem-CatChem 13:4010–4018. https://doi.org/10.1002/CCTC.202100602
- Wang D, Chen C, Wang J et al (2016) High thermal conductive core-shell structured Al2O3@Al composite supported cobalt catalyst for Fischer-Tropsch synthesis. Appl Catal A Gen 527:60–71. https://doi.org/10.1016/J.APCATA.2016.08.027
- Toshima N (2000) Core/shell-structured bimetallic nanocluster catalysts for visible-light-induced electron transfer. Pure Appl Chem 72:317–325. https://doi.org/10.1351/PAC200072010317/ MACHINEREADABLECITATION/RIS
- Mohammad N, Aravamudhan S, Kuila D (2022) Atomic layer deposition of cobalt catalyst for Fischer-Tropsch synthesis in silicon microchannel microreactor. Nanomaterials 12:2425. https:// doi.org/10.3390/NANO12142425/S1

Publisher's Note Springer Nature remains neutral with regard to jurisdictional claims in published maps and institutional affiliations.

Springer Nature or its licensor (e.g. a society or other partner) holds exclusive rights to this article under a publishing agreement with the author(s) or other rightsholder(s); author self-archiving of the accepted manuscript version of this article is solely governed by the terms of such publishing agreement and applicable law.

